Full title: **Starvation resistance in the nematode *Pristionchus pacificus* requires a conserved supplementary nuclear receptor**

Short title: **NHR-10 is required for starvation resistance in *P. pacificus***

Tobias Theska, Tess Renahan, and Ralf J. Sommer*

Max Planck Institute for Biology, Tübingen,
Department for Integrative Evolutionary Biology,
Max-Planck-Ring 9,
72076 Tübingen, Germany

***Corresponding author**

Ralf J. Sommer (ralf.sommer@tuebingen.mpg.de)

ORCIDs

Tobias Theska - https://orcid.org/0000-0002-0920-4427
Tess Renahan - https://orcid.org/0000-0002-4326-0254
Ralf J. Sommer - https://orcid.org/0000-0003-1503-7749

Keywords

nuclear receptor, phenotypic plasticity, starvation resistance, ortholog conjecture, nematode, *Pristionchus pacificus*

Abstract

Nuclear hormone receptors (NHRs) are a deeply-conserved superfamily of metazoan transcription factors, which fine-tune the expression of their regulatory target genes in response to a plethora of sensory inputs. In nematodes, NHRs underwent an explosive expansion and many species have hundreds of *nhr* genes, most of which remain functionally uncharacterized. However, recent studies elucidated that two sister receptors, *Ppa*-NHR-1 and *Ppa*-NHR-40, are crucial down-stream regulators of feeding plasticity in the diplogastrid model organism *Pristionchus pacificus*. In this study, we functionally characterize *Ppa*-NHR-10, the closest paralog to *Ppa*-NHR-1 and *Ppa*-NHR-40, aiming to demonstrate that it too regulates aspects of feeding plasticity. We used CRISPR/CAS9-mediated mutagenesis to create knock-out mutations of this receptor and applied a combination of geometric morphometrics and unsupervised clustering to characterize potential mutant phenotypes. Surprisingly, we found that *Ppa*-NHR-10 is not involved in the regulation of plasticity in feeding structures. Instead, multiple RNA-seq experiments revealed that many of the target genes of this receptor are crucial for lipid catabolism. We hypothesized that their mis-regulation could affect the survival of mutant worms during starvation, where lipid catabolism is often essential. Using survival assays, we found that mutant worms indeed show drastically decreased starvation resistance, both as young adults and as dauer larvae. We also characterized genome-wide changes to the transcriptional landscape in *P. pacificus* when exposed to 24hrs of acute starvation, and found that *Ppa*-NHR-10 partially regulates some of these responses. Taken together, we were able to demonstrate that *Ppa*-NHR-10 is broadly required for starvation resistance and regulates different biological processes than its closest paralogs *Ppa*-NHR-1 and *Ppa*-NHR-40 and its one-to-one ortholog in *Caenorhabditis elegans.* This shows that, amongst distantly-related model nematodes, even deeply-conserved NHRs can regulate vastly distinct biological processes and that neither paralogs, nor one-to-one orthologs, may be adequate predictors of their biological functions.

Author summary

When predicting the biological function of a gene (or the protein it encodes) we usually use its homologs for reference since it is likely that our gene or protein of interest has homologs in a different organism (orthologs) or in the same organism (paralogs), whose biological roles have already been characterized via molecular genetic interventions. However, predicting biological functions from homologs can have its limitations. In this study, we functionally characterized a conserved nuclear receptor, *Ppa*-NHR-10, in the nematode *Pristionchus pacificus* and found that both dauer larvae (a specialized dispersal stage) and adult worms are less resistant to starvation if this receptor is experimentally rendered non-functional. Not only did these findings reveal that *Ppa*-NHR-10 is crucial for the worms to survive harsh conditions they would frequently encounter in the wild, they also demonstrated that *Ppa*-NHR-10's homologs would not have been adequate predictors of its biological role: its homolog in *Caenorhabditis elegans* regulates a metabolic shunt pathway; its paralogs in *P. pacificus* regulate feeding plasticity. Thus, our data suggests that conserved nuclear receptors can functionally diversify across distantly-related nematodes, and that we cannot categorically infer their biological roles from well-studied homologs.

Introduction

Nematodes are an incredibly abundant and stunningly diverse group of roundworms, which occupy nearly all ecosystems across the globe. Recent estimates predict that they make up approximately 80% of all terrestrial animals [1] and that the number of unnamed species ranks in the millions [2,3]. Historically, nematodes, especially *Caenorhabditis elegans*, have been used by cell biologists to unravel fundamental secrets of animal physiology, metabolism, and cell fate [4-8], and by developmental biologists to dissect the essential processes of animal ontogeny, including heterochrony, developmental systems drift, and phenotypic plasticity [9-14].

Phenotypic plasticity, the ability of a single genotype to produce different phenotypes depending on the environmental cues that the organism receives during development, has re-gained wide-spread attention as a crucial driving force in organismal evolution [15], especially in the context of contemporary debates surrounding a proposed extension of standard evolutionary theory [15-18].

Diplogastrid nematodes such as *Pristionchus pacificus* and its conspecifics are model organisms used to study the molecular mechanisms that govern phenotypic plasticity and the role it plays in phenotypic evolution [12,18-20]. These worms display a morphological novelty in their mouths that renders them unique amongst roundworms: they possess movable cuticular teeth which allow them to predate on other nematodes (Fig 1A). This phenotype is plastic; depending on the environment, one of two alternative adult morphologies can be adopted: the predatory "eurystomatous" morph which has two cuticular teeth, or the strictly bacterial-feeding "stenostomatous" morph that only has a single tooth (Fig 1A) [12]. Recent studies utilizing *P. pacificus* began to elucidate the complex genetics behind this dimorphism [12,21-23] and identified two transcription factors, *Ppa*-NHR-1 and *Ppa*-NHR-40, as crucial down-stream regulators in the gene regulatory network (GRN) that governs mouth-form plasticity [24]. While these NHRs constitute important regulatory elements of the plasticity GRN, new molecular players continue to be found on a regular basis [25-27], expanding our knowledge of this genetic network and how it evolved along with the morphologically novel teeth.

Another plastic phenotype maintained in *P. pacificus,* and most nematodes, is related to their life cycles. Under suboptimal environmental conditions, e.g. overcrowding or food depletion, young larvae can enter an indirect life cycle (Fig. 1B) as dauers, an arrested developmental stage [28,29]. Dauers are specialized non-feeding larvae adapted for stress survival [6,28] and dispersal [30]. Characteristic morphological features of dauers include a thickened body wall cuticle and a closed buccal cavity with a plug clogging the alimentary channel (Fig 1C). Once environmental conditions turn more favorable, the worms can exit dauer and resume development into reproducing adults (Fig 1B). Interestingly, as in mouth-form plasticity, NHRs play important roles in regulating dauer plasticity [29,31].

NHRs - nuclear (hormone) receptors - constitute one of the most important transcription factors classes in animals, in which they integrate cellular metabolism with physiological function [32]. These transcription factors are restricted to metazoans [33] and they generally share an archetypical protein domain organization. Their two most important domains are the DNA-binding domain (DBD), which recognizes specific DNA motifs in the *cis*-regulatory regions of their regulatory target genes, and the ligand-binding domain (LBD), which regulates the activity state of the NHR depending on the presence or absence of a specific ligand [32,33].

125 Recent advances in genomics revealed that nematodes, in contrast to other animals,
126 often possess hundreds of *nhr* genes [24,34]. The overwhelming majority of these, called
127 "supplementary nuclear receptors" (*supnrs*), originated from an explosive burst of
128 duplications of the nuclear receptor HNF4 [35,36]. Another striking observation among
129 distantly-related nematodes with similarly high numbers of NHRs (e.g. *C. elegans* [n=266]
130 and *P. pacificus* [n=254]) showed that the vast majority of NHRs is completely lineage-
131 specific with no one-to-one orthologs in other species [24]. Additionally, the expression of
132 *supnr* genes in the nervous system is highly biased toward sensory neurons [34], suggesting
133 that the expansion of NHRs, which is particularly blatant in free-living nematodes [34],
134 could be linked to the worm's complex sensory environments filled with entangled
135 microbial foods. Here, *supnrs* might act as sensors of environmental food signals or internal
136 metabolic signals derived from ingested bacterial food, and may adjust the worm's
137 physiological states or behavioral responses according to perceived environmental
138 information [34], an idea that has recently been demonstrated for a *supnr* in *C. elegans* [37].
139 Intriguingly, *Ppa-nhr-1* and *Ppa-nhr-40*, the aforementioned mouth-form plasticity
140 regulators in *P. pacificus*, are representatives of these nematode-specific *supnrs* [24]. Yet, they
141 are two of the very few *supnrs* which are actually conserved across distantly-related species.
142 A previous study demonstrated that they co-regulate a group of fast-evolving genes
143 encoding enzymes needed for the turnover of the cuticular material that makes up the
144 worm's teeth [24]. The same study also included a phylogeny of the NHRs found in *C.*
145 *elegans* and *P. pacificus*. Interestingly, this phylogeny indicated that one more NHR, *Ppa*-
146 NHR-10, might be another deeply-conserved *supnr* and the potential sister receptor to *Ppa*-
147 NHR-1 and *Ppa*-NHR-40. If this were true, we speculated, *Ppa*-NHR-10 could be another
148 important mouth-form plasticity regulator that was hitherto overlooked.
149 Thus, we set out to investigate the biological function of P*pa*-NHR-10, using an
150 integrative approach that combines CRISPR-mediated knockouts of this receptor, geometric
151 morphometric analyses of mutant mouth morphologies, and regulatory-target
152 identification via transcriptomics. Surprisingly, our data demonstrated that *Ppa*-NHR-10 is
153 not involved in regulating mouth-form plasticity, but that it is required for the survival of
154 acute starvation in young adults and long-term starvation in dauer. We also elucidated
155 genome-wide patterns of transcriptional responses to acute starvation in *P. pacificus* and
156 found that NHR-10's regulatory targets include multiple enzymes involved in lipid
157 catabolism and transport, some of which are starvation-response genes (SRGs).

Results

Ppa-NHR-10 is a deeply-conserved supplementary nuclear receptor and the closest relative of *Ppa*-NHR-1 and *Ppa*-NHR-40

We first aimed to investigate whether *Ppa*-NHR-10 is indeed a member of the supplementary nuclear receptor cluster that includes *Ppa*-NHR-1 and *Ppa*-NHR-40, as indicated in the two-species NHR phylogeny in Sieriebriennikov *et al.* [24]. For this, we searched for orthologs of these three receptor proteins across different nematode species, based on which we aimed to reconstruct their phylogeny. We decided to include a total of ten species, representing members of clades III-V, in our analysis. We also expanded the number of representative species in Diplogastridae and Rhabditidae, as this allows a more nuanced reconstruction of the evolution of this small NHR-cluster in these families.

We found that these three NHRs indeed form a cluster of *supnrs* that is deeply conserved across the investigated nematode clades and that, usually, each species has exactly one copy of each of these receptors encoded in their genome (Fig 1D). Notable exceptions to this observation are *Brugia malayi*, which seems to lack an ortholog of NHR-10, and *Haemonchus contortus*, which lacks a copy of NHR-40 but has two copies of NHR-10. We were also able to confirm previous results [24] which suggested that NHR-1 and NHR-10 are sister receptors, and that NHR-40 is their next closest relative. Lastly, our maximum likelihood tree suggests that NHR-68, NHR-101, and NHR-114 form a group of supplementary receptors that evolved via multiple gene duplications in the lineage leading to *Caenorhabditis* nematodes. Thus, these receptors lack any one-to-one orthologs in the other investigated nematode species. In contrast, one-to-one orthology across species could clearly be established for NHR-1, NHR-10, and NHR-40 (Fig 1D).

These results suggest that, although these three NHRs represent nematode-specific *supnrs*, they were conserved across at least 130 million years of evolution [38]. This is stunning, as the vast majority of these receptors is entirely lineage-specific, undergoing rapid evolutionary turnover [24]. Additionally, NHR-10 is deeply nested within this cluster and, in *P. pacificus*, it is the last remaining one among these three receptors for which the biological function remains unknown. We hypothesized that *Ppa*-NHR-10 is likely another regulator of this plasticity and that, probably, the entire NHR-1/-10/-40 cluster was co-opted into this functional context during diplogastrid evolution. To further investigate this possibility, we wanted to study the cellular expression patterns of *Ppa-nhr-10*.

Ppa-nhr-10 is expressed in multiple tissues including the hypodermis, pharyngeal glands, uteri, spermathecae, and rectal glands

Previous studies from our lab demonstrated that *Ppa-nhr-1* and *Ppa-nhr-40* are co-expressed in the pharyngeal muscles, the tissues that produce the cuticular teeth of *P. pacificus* [24]. Additionally, all of their joint regulatory targets show an incredibly consistent expression pattern in a single cell: g1D. This is a gland cell of *P. pacificus*, which is morphologically integrated with the dorsal pharynx, where it runs through the dorsal tooth and opens into the mouth lumen [39]. Thus, we anticipated to find *Ppa*-NHR-10 to be expressed in any of these tissues.

Our transcriptional reporter animals revealed that *Ppa-nhr-10* is expressed in a variety of tissues (Fig 2). These always included the skin of the worms (hypodermis) (Fig 2A, 2B, and 2C), the anterior and posterior uteri and spermathecae (Fig 2A, 2B, and 2D), the

rectal glands (Fig 2A), and, expectedly, the pharyngeal glands (Fig 2A and 2C). While all of our worms consistently showed an expression in all three of the pharyngeal gland cells (g1D, g1VL, g1VR) [39], the relative intensity of the expression signal varied across the two independently acquired reporter lines: in one reporter line the ventral pharyngeal glands (g1V) dominate the signal (Fig 2A), while in the other the dorsal pharyngeal gland (g1D) reports more strongly (Fig 2B and 2C). Additionally, one of the lines only shows a weak expression pattern in the rectal glands (Fig 2A *vs.* 2B). Thus, the reported expression patterns were, at least partially, in line with our expectations.

Taken together, the fact that *Ppa-nhr-10* is the deeply conserved paralog of *Ppa-nhr-1* and *Ppa-nhr-40*, and that it is expressed in the same tissues (and/or their regulatory targets), indicated to us that this *supnr* may indeed be another member of the plasticity-regulating network in *P. pacificus*. Thus, we set out to characterize whether the loss of *Ppa-nhr-10* would lead to any mouth-form plasticity related mutant phenotypes.

Loss of *Ppa-nhr-10* does not affect stoma morphology and only weakly affects mouth-form plasticity

We created multiple independent *loss-of-function* alleles of *Ppa-nhr-10* (genome annotation: El Paco v3, gene_ID: PPA01780, chromosome: ChrIII). We used CRISPR/CAS9 to introduce frameshift mutations into the gene body that would disrupt and truncate the nuclear receptor protein either at the site of the DNA-binding domain (DBD) or the ligand-binding domain (LBD). While we were unable to obtain viable frameshift alleles in the DBD, we succeeded in independently generating four homozygous mutant lines with frameshifts truncating the LBD (crRNA sequence: GGCGCGTGGGTTCGGGCGTA; PAM: CGG). Two of these lines were chosen to establish the *Ppa-nhr-10(lof)* reference strains RS3920(*tu1654*) and RS3921(*tu1655*), which we used for all subsequent experiments in this study (Fig 3A).

Next, we wondered whether our *Ppa-nhr-10* mutants display any morphological phenotypes related to mouth-form plasticity, just as *Ppa-nhr-1* and *Ppa-nhr-40* mutants do [22,24]. We found that both *Ppa-nhr-10* mutant strains show a detectable decrease in the number of predatory morphs when compared to wild-type worms (Fig 3B). While this effect is well supported by our data (wildtype *vs.* RS3920: $Z = 2.1$, $P = 0.0058$; wildtype *vs.* RS3921: $Z = 2.6$, $P = 0.0004$) and consistent across both mutant strains (RS3920 vs. RS3921: $Z = 0.05$, $P = 0.4839$), it is only marginal in size (~ 4-5%). This is in stark contrast to the effects observed for *loss-of-function* and *gain-of-function* mutations in *Ppa-nhr-40,* which lead to a complete loss of the predatory or bacterivorous morphs, respectively. Given the small size of the effect that *Ppa-nhr-10* mutations exert on the worm's morph ratio, and taking into account the vast diversity of factors influencing the mouth-form decision [12,18,27], we concluded that *Ppa-nhr-10* is unlikely to be a direct regulator of mouth-form plasticity. Indeed, it seems more likely that the small observed effects on the morph ratio are indirect consequences of the misregulation of *Ppa-nhr-10*'s true regulatory target pathways.

Additionally, we found that the loss of *Ppa-nhr-10* does not affect the overall morphology of the adult mouth. A geometric morphometric analysis 2-dimensional landmark data from 144 individual worms (48 per strain) showed very homogenous and highly overlapping ranges of morphological variation in mouth form across wild-type worms and *Ppa-nhr-10* mutants (Fig 3C). A principal component analysis (PCA) of our form data revealed that, together, PC1 and PC2 capture the majority of form variation in the data (60.2%). Additionally, we were able to estimate that PC1 and PC2 are the only "meaningful" principal components *sensu* Schlager et al. [40,41] and that the other PCs are likely to contain

noise rather than signal. Subsequent model-based clustering of all individuals in the form dataset (based on the information contained in the "meaningful" PCs) revealed that mutant worms could not be classified as such, or differentiated from wild-type worms, based on their mouth morphologies alone (Fig 3D). Together, our geometric morphometric and model-based clustering analyses support the absence of any discernible mutant phenotypes in the mouth of *Ppa-nhr-10* mutants. Again, these findings are in blatant contrast to the phenotypes caused by the loss *Ppa-nhr-1,* which leads to structural alterations of the mouth and gives rise to worms with an intermediary mouth morphology combining anatomical features of predators and bacterivors [24].

Taken together, the results of our morphological analyses do not support our initial hypothesis that *Ppa*-NHR-10 is another constituent of the gene regulatory network that governs mouth-form plasticity in *P. pacificus*. This also indicates that not the entire NHR-1/-10/-40 cluster was co-opted into said functional context during diplogastrid evolution. Intrigued by this observation, we set out to elucidate the biological function of NHR-10 in *P. pacificus,* starting with exploratory RNA-seq experiments.

Exploratory transcriptomics suggests *Ppa*-NHR-10 might be a regulator of lipid catabolism and transport

Since nuclear receptors are transcription factors, it is possible to identify their potential regulatory target genes, and thus infer their potential biological functions, through comparative transcriptomics. We analyzed the transcriptomes of wild-type worms (PS312), and *Ppa-nhr-10(lof)* mutants (RS3920 and RS3921) at two developmental stages (larvae and adults). We aimed to identify potential "core targets" of *Ppa*-NHR-10 which we considered to be genes that are consistently mis-regulated (i.e., differentially expressed) in both mutant strains, in at least one of the two developmental stages.

In doing so, we were able to identify 32 potential regulatory target genes, of which 25 were down-regulated and seven up-regulated (Fig 4). We found 11 genes consistently differentially expressed in mutant larvae and 12 in mutant adults (compared to their wild-type counterparts). The larval targets include multiple down-regulated collagens and up-regulated proteins which are known to be involved in stress responses, like C-type lectins or the UDP-glycosyltransferases (Fig 4). Interestingly, we also found two proteins, both of them strongly down-regulated, which are predicted to be involved in the binding and transport of lipids: PPA13553 (an ortholog of the *C. elegans* vitellogenin *vit-6*) and PPA05630 (a predicted apolipoprotein). On the other hand, all of the 12 targets we identified in adult mutants were down-regulated and they include a more diverse array of proteins, ranging from a membrane-trafficking protein (PPA08133/*Ppa-scm-1*), to a component of the RNA polymerase II complex (PPA14053/*Ppa-lin-25*), to a chromatin organization modifier (ppa_stranded_DN31598_c1_g4_i2), to one of the TGF-β signaling receptors (PPA15180/*Ppa-daf-4*). The latter is particularly interesting, as TGF-β signaling in *C. elegans* is involved in both the formation of the dauer larvae and the regulation of body fat [42,43].

Strikingly, we found nine putative target genes which are strongly and constitutively mis-regulated across both developmental stages in *Ppa-nhr-10(lof)* mutants, and the majority of them have predicted functions in lipid catabolism. Briefly, canonical lipid catabolism involves three processes: (I) lipolysis - the cleavage of neutral storage lipids (TAGs) into glycerol and free fatty acids by lipases, (II) activation - the ligation of CoA to free fatty acids by fatty acyl-CoA synthetases (ACSs), and (III) β-oxidation - the breakdown of activated fatty acids into acetyl-CoA molecules. The latter process is generally performed in four

298 steps: dehydrogenation by acyl-CoA dehydrogenases (ACDHs), hydration by enoyl-CoA
299 hydratases (ECHs), dehydrogenation by 3-hydroxyacyl CoA dehydrogenases (3-HACDs),
300 and thiolytic cleavage by thiolases [5,43,44]. Most excitingly, the constitutively mis-
301 regulated putative targets of *Ppa*-NHR-10 include two predicted lipases (PPA07082 and
302 Iso_D.954.1), two predicted ACSs (PPA05769 and PPA13813), as well as a predicted ECH
303 (PPA40903). Furthermore, these genes are among the most strongly affected by the loss of
304 *Ppa-nhr-10.* This is reflected in the fact that they show some of the largest L2FC-estimates
305 among all putative regulatory targets (Fig 4).
306 Taken together, our exploratory transcriptome and differential expression analyses
307 suggest that *Ppa*-NHR-10 might be an important regulator of body fat in *P. pacificus.* This is
308 evident in the observation that the loss of *Ppa-nhr-10* negatively affects the expression of
309 genes predicted to be involved in all the major processes of lipid catabolism, as well as genes
310 encoding proteins required for the transport of lipids across tissues. Given that lipid
311 metabolism and life span are tightly linked in all animals [45], and knowing that functional
312 interferences with any of the lipid catabolic processes in nematodes can impair their
313 survival capabilities across various environmental conditions [43,44], we decided to
314 quantify the survival capabilities of our *Ppa-nhr-10(lof)* mutants in different conditions,
315 expecting to find that they are unlike those of wild-type worms.
316

317 **Survival analyses reveal that *Ppa-nhr-10* is required for survival of acute starvation in**
318 **young adults**

319 In *C. elegans*, interference with the major lipid catabolic pathways can lead to altered life
320 spans and/or rates of survival over time. While some mutations in these pathways
321 constitutively impair the worm's survival capabilities, irrespective of environmental factors,
322 others are known to cause such impairments only in certain conditions like starvation [43-
323 45]. Minding these details, we decided to examine the survival capabilities of wild-type *P.*
324 *pacificus* and *Ppa-nhr-10(lof)* mutants in two different conditions: well-fed and acutely-
325 starved. To achieve this, we transferred young adult hermaphrodites into small cell culture
326 flasks which either contained a standard liquid culture (LC) medium rich in OP50, or a LC
327 medium that contained no food. To obtain the survival curves, we scored the number of
328 survivors every 24hrs until all worms in the flasks were dead.
329 First, we found that the obtained time-to-death data from the well-fed condition is
330 compatible with the hypothesis that there are no differences in the overall survival
331 capabilities of *Ppa-nhr-10(lof)* mutants and wild-type worms (Fig 5A and 5C). Neither the
332 global Kaplan-Meier (K-M) survival analysis of well-fed worms (Fig 5C: $\chi^2 = 5.7$, $P =$
333 0.060431), nor the pairwise comparisons of strain-specific survival curves via a log-rank test,
334 revealed any significant differences in survival (Fig 5A). Yet, we found that hazard ratios
335 were estimated to be slightly elevated in the mutant strains compared to the wild-type level
336 of 1.0 (1.15 for RS3920 and 1.13 for RS3921). However, while these hazard ratios do equate
337 to a ~15% increase in the relative risk of death at any given timepoint in the experiment,
338 these estimates were still found to be compatible with the null hypothesis given their
339 associated uncertainty (Fig 5C).
340 Remarkably, we found the exact opposite to be true for our starvation experiments:
341 the global K-M analysis indicated stark differences in the overall survival probabilities
342 among starving worms (Fig 5C: $\chi^2 = 175$, $P = 1.51e\text{-}38$) and the log-rank pairwise
343 comparisons revealed that the survival curves of both *Ppa-nhr-10(lof)* mutants, while being
344 virtually identical to each other (Fig 5B: $P = 1.0$), differed markedly from the wild-type

survival curve (Fig 5B: $P < 2e\text{-}16$). Additionally, we found highly elevated hazard ratios for the *Ppa-nhr-10(lof)* mutants compared to wild-type *P. pacificus* (Fig 5C: 2.23 for RS3920 and 2.12 for RS3921). Simply, these estimates mean that for every wild-type worm that dies at any given point of time during the starvation experiment, more than two mutant worms will face the same fate. These large effects are incompatible with our null hypothesis (P[RS3920]= 4.79e-30 and P[RS3921]= 3.91e-27) and strongly support decreased survival rates in mutant worms (Fig 5C).

Taken together, our condition-specific survival experiments revealed that acute starvation induces highly elevated rates of premature deaths in young adult worms which lack a functional copy of *Ppa-nhr-10*. While this observation confirmed the hypothesis we formulated based on our exploratory RNA-seq results, one might now want to argue that, given the condition-specificity of the identified phenotype, our initial sequencing approach was, in fact, not ideal. This is because all the worms we used for the exploratory RNA-seq analysis were well-fed rather than starved. This means that, amongst all of the identified putative targets which potentially cause the survival phenotype in starving mutants, the exploratory analysis could have picked up only on those genes which are constitutively mis-regulated (i.e., in well-fed *and* acutely-starved conditions). Therefore, we potentially missed out on a pool of putative target genes, which are mis-regulated in mutants specifically *in response to* starvation. Obviously, such genes would be important to explain the starvation-specific survival phenotypes and, if they exist, this could argue that *Ppa*-NHR-10 itself is a regulator of the starvation-response machinery in these nematodes. In order to expand our analysis as to include genes that are mis-regulated in mutants responding to starvation, and to elucidate whether any of *Ppa*-NHR-10's putative targets are members of the worm's starvation-response machinery, we performed confirmatory RNA-seq experiments which included both, well-fed and acutely-starved, wild-type and mutant worms from our LC set-up.

Starvation induces substantial transcriptional responses in genes predicted to be involved in metabolism, stress responses, and translation

To begin with, we aimed to elucidate genome-wide changes to the transcriptional landscape in wild-type worms which faced 24hrs of acute starvation. Using our differential expression pipeline, we were able to identify a total of 1,007 genes showing a response to starvation (Fig 6A). Of these, 294 genes were notably up-regulated (cluster I in Fig 6) and 713 notably down-regulated (cluster II in Fig 6). Thus, our data shows, for most of these starvation-responsive genes (SRGs), the worms strongly decrease expression levels compared to when food is abundantly available.

Next, we wondered what kinds of genes are up- or down-regulated. Are the SRGs predominately diplogastrid-specific orphan genes, or phylogenetically old? Are they members of any known co-expression modules? What kind of proteins do they encode and are there biases towards specific protein classes responding to starvation? Lastly, do the SRGs fall into any specific biological pathways? To address these questions, we mined a wealth of available data through overrepresentation analyses (ORAs).

First, we found that phylogenetically old genes, rather than diplogastrid-specific orphans, are overrepresented in both SRG clusters (Fig 6B). While these observed effects are well-supported by our data (q[cluster I] = 3.7e-04 and q[cluster II] = 1.8e-05), their sizes are comparatively small (fold enrichment: cluster I = 1.15 and cluster II = 1.12). However, while

391 they do constitute the minority of SRGs, there are still hundreds of orphan genes
392 functionally responding to starvation (Fig 6B).
393 Next, we asked whether any of the co-expression modules that were recently
394 identified in a nutrigenomic study [46] were overrepresented among the SRGs. Indeed,
395 genes which belong to the modules "oogenesis 3", "nervous system 2", "nervous system 3",
396 and "nervous system 5" where strongly enriched amongst the up-regulated SRGs. On the
397 other hand, members of the co-expression modules "orphan 3", "cuticle 1", "nervous system
398 4", "intestine 1", "intestine 3", and "intestine 4" where strongly enriched among the down-
399 regulated SRGs (Fig 6B).
400 To identify the potential biological functions of the SRGs, we predicted the types of
401 protein domains (PFAM [47]) that they encode and, additionally, we functionally annotated
402 the SRGs with WormCat (ver. 2) terms [48] wherever a single ortholog was available in *C.*
403 *elegans*. Amongst the up-regulated SRGs, there is a clear bias towards genes that encode
404 proteins which are critical for the translational process and protein synthesis (Fig 6C). This
405 includes large ribosomal subunit proteins (Ribosomal_L6e), elongation factors (GTP_EFTU,
406 GTP_EFTU_D2), and tRNA synthetases (tRNA-synt_1, tRNA-synt_1c). This pattern was
407 further confirmed by our ORA of WormCat terms, which found only a single major category
408 enriched among the up-regulated SRGs: "Ribosome" (Fig 6D). This category contains genes
409 that encode proteins and RNA which constitute, assemble, or regulate the ribosome and
410 translational processes [48]. Within the ribosome category, we further found an
411 overrepresentation of genes belonging to the "biogenesis" subcategory (q = 1.1e-07), which
412 encode proteins acting in ribosome assembly [48] (Fig 6D).
413 Genes which are down-regulated in response to acute starvation seem to execute
414 entirely different biological functions. We found a clear bias towards genes that encode
415 proteins involved in diverse metabolic pathways (q = 2.4e-11), as well as stress responses (q
416 = 1.7e-05) (Fig 6D). The strongest detected metabolic signal was found for lipid metabolism
417 (q = 9.3e-11), followed by amino acid metabolism (q = 6.7e-07), and the one-carbon cycle (q
418 = 0.0203). We further detected overrepresentation signals for specific aspects of these
419 individual metabolic pathways. This includes genes which encode proteins involved in the
420 elongation and desaturation of fatty acids ("fatty acid"), lipid binding, as well as in the
421 breakdown and synthesis of amino acids, and the conversion of homocysteine to
422 glutathione ("transsulfuration") [48] (Fig 6D). The strong overrepresentation pattern for
423 lipid metabolic pathways, was further corroborated by our ORA of PFAM domains, which
424 revealed strong enrichments for lipases (Lipase_GDSL, Lipase_GDSL_2), fatty acid
425 elongases (ELO), fatty acid desaturases (FA_desaturase), and lipid-binding vitellogenins
426 (Vitellogenin_N) (Fig 6C). The second-most overrepresented functional category among
427 down-regulated SRGs - stress response - is based on the presence of multiple C-type lectins,
428 p450 cytochromes, and lysozymes in cluster II (Fig 6C and 6D). These genes are involved in
429 the worm's immune response, the detoxification of xenobiotic compounds, and the survival
430 of pathogenic stresses, respectively [48].
431 Taken together, irrespective of the direction of the effect, genes which
432 transcriptionally respond to acute starvation are mostly phylogenetically old (Fig 6B).
433 Interestingly, genes which are up-regulated during starvation are predominantly members
434 of various nervous system and oogenesis related co-expression modules, and they tend to
435 encode proteins that are crucial constituents of the translational machinery. In contrast,
436 genes that are down-regulated in response to starvation are predominantly members of
437 various intestinal co-expression modules and tend to encode proteins that are crucial

enzymes in lipid and amino acids metabolism, as well as important detoxification and immune response elements (Fig 6).

With this reference knowledge of genome-wide patterns of starvation responses in hand, we next set out two analyze the transcriptomes of starved *Ppa-nhr-10(lof)* mutants to see which genes are likely to explain the starvation-induced survival phenotype, and whether any of them are members of the identified SRGs.

Confirmatory transcriptome analyses indicates that *Ppa*-NHR-10 regulates aspects of the wild-type starvation response, lipid metabolism, and TGF-β signaling

Our confirmatory transcriptome analysis revealed a majorly updated list of 37 putative *Ppa*-NHR-10 targets, of which 32 were down-regulated and five up-regulated (Fig 7). To validate that these statistically inferred candidate genes are indeed appropriate to address our questions, we submitted their *rlog*-transformed [49] normalized count values to unsupervised hierarchical clustering. Ideally, these candidate genes should capture the information needed to differentiate well-fed from starved, and wild-type from mutant worms. Thus, the clustering algorithm should be able to recover these experimental groupings from the candidate gene data alone. This was indeed the case (Sup Fig 1), confirming that our improved list of putative regulatory targets is appropriate to address the observed starvation-survival phenotype in mutant worms, and to identify any putative targets that are starvation-responsive (i.e., SRGs).

As expected, our original exploratory RNA-seq experiments missed a majority of putative causal targets (28 out of 37). Unfortunately, many of the newly identified target genes have a wide variety of predicted functions which are not easily grouped into overarching processes (Fig 7). Strikingly, however, we recovered nine of the putative *Ppa*-NHR-10 targets that were already found in the exploratory analysis (Fig 4 and Fig 7), including the TGF-*β* receptor PPA15180/*Ppa-daf-4,* the p450 cytochrome PPA25752/*Ppa-cyp-33B1*, and the two lipid catabolic enzymes PPA05769/*Ppa-acs-14* and PPA40903 (Fig 4 and Fig 7). This confirms that, while our initial RNA-seq approach was not ideal, it was still able to identify some of the putative phenotype-causing targets of *Ppa*-NHR-10.

More importantly, our confirmatory RNA-seq approach did actually confirm the initially observed pattern: a bias toward regulatory targets that are involved in the transport and break of lipids and fatty acids (Fig 7). PPA33234/*Ppa-strl-1* is a lipid-binding protein predicted to be located in mitochondria and involved in the transport of cholesterol for steroid biosynthesis. PPA27650 is predicted to be involved in intermembrane transport of lipids as part of glycerolipid synthesis. Genes that encode important players in the *β*-oxidation of fatty acids were recovered, too: PPA05769/*Ppa-acs-14* is a fatty acyl-CoA synthetase, the type of enzyme that "activates" free fatty acids for *β*-oxidation. Additionally, the gene *ppa_stranded_DN29959_c0_g2_i3* encodes an acyl-CoA dehydrogenase (ACDH) and PPA40903 an enoyl-CoA hydratase (ECH). These two enzymes catalyze the first two of the four canonical steps in mitochondrial *β*-oxidation [43-45].

Lastly, we wondered what the gene regulatory basis of the starvation-survival phenotype in *Ppa-nhr-10(lof)* mutants looks like and anticipated two different scenarios. One, that NHR-10's regulatory targets would be members of genetic networks which are not part of the starvation response machinery (Fig 6), but might, when mis-regulated, lead to decreased survival capabilities in mutant worms that face starvation. Alternatively, *Ppa*-NHR-10's regulatory targets could actually constitute members of the SRGs. In this latter scenario, the impaired survival capabilities of starving mutants would be directly explained

485 by malfunctions in the starvation-response machinery itself. Surprisingly, our analysis
486 suggested a combination of both: while the majority of putative *Ppa*-NHR-10 targets are
487 genes that do not respond to starvation, we were still able to identify four SRGs among them
488 (Fig 7). Strikingly, these four SRG targets included the two aforementioned β-oxidation
489 enzymes (ACDH and ECH), of which one was already found in our exploratory RNA-seq
490 analysis; an observation that also applies to another SRG target: the p450 cytochrome
491 PPA25752/*Ppa-cyp-33B1* (Fig 7).
492 Taken together, this new data corroborated our original hypothesis that *Ppa*-NHR-10
493 controls general aspects of fatty acid breakdown and, additionally, demonstrated that this
494 supplementary nuclear receptor is required for some of the worm's transcriptional
495 responses to acute starvation.
496

497 **Dauer assays demonstrate that the loss of *Ppa-nhr-10* also affects dauer entry rates,**
498 **dauer exit speed, and long-term dauer survival**

499 Finally, we wondered whether *Ppa*-NHR-10 might play a more general regulatory role in
500 starvation survival beyond its requirement for starvation resistance in young adult worms.
501 Thus, we investigated the potential effects that the loss of this receptor might have on a
502 different life history stage: dauer larvae (Fig 1B). We hypothesized to see effects on dauers
503 for multiple reasons: First, they represent the worm's natural state of starvation, as their
504 buccal plugs prevent them from taking in any food (Fig 1C) [6,28]. Second, it is well
505 established that dauer metabolism in *C. elegans* is heavily dependent on the generation of
506 energy from stored neutral lipids via lipolysis and fatty acid β-oxidation [50-53]. Third, it is
507 known that various NHRs are involved in the regulation of dauer entry, dauer exit, and
508 metabolism [31,42-44]. Taking all these factors together, while integrating our findings that
509 *Ppa*-NHR-10 is required for starvation survival in young adults and that it seems to regulate
510 some of the very aspects of lipid breakdown, which also constitute the foundation of dauer
511 metabolism, we were optimistic to find alterations in dauer larvae of our mutant worms.
512 We quantified three different aspects of dauer biology: i) the number of worms which
513 entered the dauer stage due to overcrowding, ii) the time it took the worms to exit dauer
514 and resume development when re-introduced to food, and iii) the survival of dauers over
515 extended periods of time (Fig 8A).
516 Interestingly, for dauer entry, we found an allele-specific phenotype in only one of
517 our *Ppa-nhr-10(lof)* mutants: RS3920(*tu1654*). Across culture conditions, worms belonging to
518 this strain showed a decreased number of dauer larvae in the overall population when
519 compared to the wild-type and the second mutant strain (Fig 8B). However, such allele-
520 specific phenotypes could not be observed in the other dauer assays. In fact, just like in all
521 of our previous experiments, the two mutant strains behaved in an almost indistinguishable
522 manner (Fig 8C and 8D). Here, our data demonstrated that animals lacking a functional
523 copy of *Ppa-nhr-10* needed considerably more time to exit the dauer stage and resume
524 normal development (Fig 8C). Where more than 80% of wild-type worms already exited
525 dauer within the first 24hrs after being re-introduced to food, less than 5% of mutant worms
526 managed to do the same (4.6% in RS3920 and 2.9% in RS3921). Only after another 24hrs on
527 food did the mutants reach somewhat similar numbers of exited worms (70.8% in RS3920
528 and 75.0% in RS3921), at which point virtually all of the wild-type worms had resumed
529 normal development (99.2% in PS312). While eventually all investigated worms completed
530 the dauer exit (and developed into fully viable adults), it took the mutants twice as long as
531 wildtype to do so (Fig 8C).

532 Excitingly, we found impaired long-term survival capabilities of mutant dauer larvae
533 (Fig 8D). Initially, after spending another week in dauer following the SDS treatment, the
534 estimated overall survival rates of wild-type and mutant dauers were indistinguishable
535 (53.5% in PS312, 56.5% in RS3920, and 52.5% for RS3921). However, this changed during the
536 second week post-SDS exposure: where wild-type worms showed estimated survival rates
537 which were indistinguishable from those of the previous week (58%), our mutant worms
538 died off rapidly, leaving almost no survivors (1.7% in RS3920 and 6.0% for RS3921) (Fig 8D).
539 This trend continued into the third week, where mutant dauers were practically extinct
540 (0.0% survivors in RS3920 and 0.3% in RS3921), while 19.3% of wild-type dauers were still
541 alive. In summary, these assays revealed that all of the investigated aspects of dauer biology
542 were negatively affected by the loss of *Ppa-nhr-10*. This observation confirmed the
543 hypothesis we conceived based on the combined results from our survival analysis and our
544 confirmatory RNA-seq data, and they demonstrate that *Ppa*-NHR-10 is indeed required in
545 the broader context of starvation resistance throughout the *P. pacificus* life cycle, including
546 the ecologically relevant dauer stage.

Discussion

In this study, we aimed to demonstrate that *Ppa*-NHR-10 is a regulator of mouth-form plasticity in *P. pacificus* and, thus, validate the hypothesis that a small but complete cluster of three closely-related and deeply-conserved supplementary nuclear receptors (*supnrs*) was functionally co-opted into the gene regulatory network that governs plasticity in the feeding structures of *Pristionchus* nematodes. We were able to demonstrate that *Ppa*-NHR-10 is indeed, amongst others, expressed in relevant tissues which are part of the morphological novelties in diplogastrid mouths (e.g., the g1D pharyngeal gland cell associated with the dorsal tooth). This is intriguing, as *Ppa*-NHR-1 and virtually all of the common regulatory targets of *Ppa*-NHR-1 and *Ppa*-NHR-40 are co-expressed in the same cell [24]. Yet, unlike mutations in the latter two receptors, loss of *Ppa*-NHR-10 neither disrupted the worm's ability to develop into predators, nor did it lead to aberrant mouth morphologies. Thus, these findings were incompatible with our initial hypothesis. Instead, our results indicate that it was specifically *Ppa*-NHR-1 and *Ppa*-NHR-40, but not the complete NHR-1/-10/-40 cluster, that were functionally co-opted when the plasticity GRN was assembled during the evolution of mouth morphological novelty in diplogastrids. This also demonstrates that the genetic basis for the evolution of plastic traits and novel structures is more complicated than often presumed, and that paralogs - at least when it comes to nematode *supnrs* - might not necessarily be adequate predictors for the functions of the genes of interest.

Through a combination of exploratory and confirmatory mRNA-seq experiments, we were able to identify *Ppa*-NHR-10's putative regulatory targets. These encompass a broad variety of proteins including many metabolic enzymes and multiple signaling elements (Fig 4 and Fig 7). Interestingly, this pattern is completely different from the regulatory target patterns of its paralogs *Ppa*-NHR-1 and *Ppa*-NHR-40: most of their targets belong to a single class of metalloproteases (astacins) that is crucial for cuticle degradation [24] and the vast majority of them is located on the X-chromosome. This is the same chromosome that also harbors *Ppa-nhr-1* and *Ppa-nhr-40*, as well as the multi-gene locus that regulates the plastic switch decision [23,24]. This pattern, again, does not hold true for the loci harboring *Ppa*-NHR-10's targets, which do not display a bias towards one particular chromosome, let alone chromosome X (Sup Tab 1). In contrast to *Ppa*-NHR-1's and *Ppa*-NHR-40's biases towards regulating a specific class of enzyme, *Ppa*-NHR-10 seems to regulate a defined biological process that involves a variety of different proteins: the activation and β-oxidation of fatty acids (Fig 4 and Fig 7). The differences in the regulatory "behaviors" among these closely-related NHRs demonstrate why, in this particular case, *Ppa*-NHR-10's paralogs were inadequate predictors of function.

Most evolutionary biologists would argue that this is not surprising and reference classical literature in the field, which teems with examples of deeply-conserved "master regulators" of development and physiology, which execute "the same" function in the most distantly related animals [54,55]. After all, they may say, orthologs are more functionally similar to one another than paralogs are [56,57]. Yet, in more recent years, researchers increasingly called into question the notion that orthologs are the better, or maybe even the only viable, homologs to turn to, if we want to predict the function of a gene of interest in a unstudied organism [58-60]. This assumption, the "ortholog conjecture" [58], so say the contenders, is no longer sustainable given the vast amount of bioinformatic evidence [59,60]. In fact, some recent studies demonstrated that paralogs can outperform orthologs in

594 functional inference tasks, and that the cumulative "big data" evidence suggests orthologs
595 and paralogs should be considered together when predicting biological functions for genes
596 of interest [60]. Thus, our example of *Ppa*-NHR-10 not being involved in mouth-form
597 plasticity, of which both of its closest paralogs are crucial regulators, is indeed surprising.
598 Stunningly, predicting *Ppa*-NHR-10's function would not have been much more
599 successful if we had looked at its well-studied one-to-one ortholog in *C. elegans* instead. *Cel*-
600 NHR-10 is known to regulate the expression levels of genes which encode enzymes that
601 constitute a nematode-specific metabolic pathway called the "propionate shunt" [61]. This
602 shunt is based on five genes (*acdh-1, ech-6, hach-1, hphd-1,* and *alh-8*), all but one of which
603 have a clear one-to-one ortholog in *P. pacificus*. While four out of five propionate shunt genes
604 in *C. elegans* show a strong mis-regulation upon NHR-10 inactivation [61], not a single one
605 of the propionate shunt orthologs in *P. pacificus* displayed altered expression levels in strains
606 that lacked a functional copy of *Ppa*-NHR-10 (Sup Tab 2). Therefore, neither the closest
607 paralogs of *Ppa*-NHR-10 (*Ppa*-NHR-1 and *Ppa*-NHR-40), nor its one-to-one ortholog in *C.*
608 *elegans* (*Cel*-NHR-10), were suitable predictors of its starvation-resistance related function
609 in *P. pacificus*. This indicates, when it comes to nematode-specific *supnrs*, that caution must
610 be exerted when assigning biological functions to receptors based on homology, rather than
611 on functional genetic investigations. In fact, the data presented in this study suggest that
612 even the very few *supnrs* which are deeply-conserved across distantly-related species might
613 regulate entirely lineage-specific functions, potentially due to rapid evolutionary turnover
614 in the acquisition of regulatory targets. Future comparative studies in *C. elegans* and *P.*
615 *pacificus* could directly test this hypothesis for other conserved *supnrs*, e.g. NHR-1 and NHR-
616 40, as their biological functions are already known in one of the species [24].
617 We also elucidated genome-wide transcriptional responses to 24hrs of acute
618 starvation in young adult hermaphrodites of *P. pacificus*. When focusing on the broad-scale
619 patterns in this data, three interesting observations emerge:
620 First, during starvation, *P. pacificus* increases the expression of numerous genes
621 which are critical elements of the translational machinery, and it decreases the expression
622 of metabolic pathway genes, especially affecting lipid transport, and the desaturation and
623 elongation of fatty acids for fat storage purposes (Fig 6C and 6D). Thus, the biological
624 pathways affected by acute starvation are consistent between *P. pacificus* and *C. elegans* [6,62-
625 64], indicating that the underlying starvation-response mechanisms are deeply conserved;
626 an observation that is also reflected in the fact that most of the SRGs are phylogenetically
627 old (Fig 6B). Yet differences exist in the details: when *C. elegans* starves, it does not change
628 the expression levels of ribosome-biogenesis genes, but it decreases the translation of their
629 transcripts [64]. We speculate that *P. pacificus* might employ a slightly different strategy, in
630 which it increases the expression of translation-related genes, while it does not increase the
631 translation of their transcripts. This way, the worms would not invest large amounts of
632 energy into the protein synthesis [6], while maintaining the ability to quickly do so if food
633 becomes available again. Once scalable proteomic methods become available for *P. pacificus,*
634 future studies will be able to directly test this hypothesis and study the evolution of these
635 molecular starvation-response strategies.
636 Second, the majority of up-regulated genes are associated with the nervous system
637 and oogenesis, while the vast majority of the down-regulated genes are associated with the
638 metabolic hub of nematodes, the intestine (Fig 6B). Additionally, we found numerous
639 down-regulated genes to be members of a co-expression module which is associated with
640 the hypodermis (Fig 6B "cuticle 1" [46]), the site of long-term lipid storage [44]. Together
641 with the observation that lipid anabolism is down-regulated during starvation, these data

642 could suggest that *P. pacificus*, when facing acute starvation as adults, might undergo drastic
643 changes to their neural regulatory landscape which may, in turn, lead the worms to switch
644 strategies from synthesizing and storing lipids to maintain their soma, to investing into egg
645 production and ensuring population survival. This would be in line with recent predictions
646 concerning neural regulation of body fat during starvation in *C. elegans* [44].
647 Third, a variety of stress responses are down-regulated in the absence of bacterial
648 food. This includes multiple proteins predicted to be involved in the detoxification of
649 xenobiotic compounds (p450 cytochromes), the immune response (C-type lectins), and the
650 defense against microbial pathogens (lysozymes) [48] (Fig 6D). This corroborates an
651 interesting observation: the uracil-auxotrophic OP50 strain of *E. coli*, the standard laboratory
652 food source for nematodes [65], might be slightly toxic to *P. pacificus* [66]. Upon ingesting
653 these bacteria, the worms may have to activate some of these stress response pathways in
654 order to be able to sustainably live off of them as a diet. Taken together, this newly-
655 established reference knowledge of responses to acute starvation complements recent
656 nutrigenomic advances [46] in *P. pacificus*, and it will inform future studies which may aim
657 to evaluate the quality of different diets. If the worm's transcriptional responses to a specific
658 bacterial food source are highly similar to the starvation responses reported in this study,
659 this could demonstrate a poor nutritional value of a given bacterial diet.
660 The present study also demonstrates that *Ppa*-NHR-10 is broadly required for
661 starvation resistance in *P. pacificus* (Fig 5 and Fig 8) and that some of its regulatory targets
662 are starvation-responsive (Fig 7). This indicates that *Ppa*-NHR-10 is one of the probably
663 many transcriptional regulators that contribute to the wild-type starvation response.
664 Interestingly, the expression levels of the *Ppa-nhr-10* gene itself do not change during acute
665 starvation (l2fc = -0.10894 and s = 0.79898), suggesting that *Ppa*-NHR-10 is already present
666 before the starvation signal is sensed. It thus seems likely that, in the context of the adult
667 starvation response, *Ppa*-NHR-10 is activated by a ligand that is present during starvation,
668 or inactivated by the absence of its ligand during starvation. Either way, future biochemical
669 studies may address the activity states of this receptor and identify its ligand. This will lead
670 to a better understanding of *Ppa*-NHR-10's role in the starvation response, and elucidate
671 how a food-depletion signal is detected and converted into a biological response via this
672 *supnr*.
673 Lastly, we found that the loss of *Ppa*-NHR-10 negatively affected multiple aspects of
674 dauer biology, using a unique method combining several assays. This allowed us to
675 investigate three pertinent dauer characteristics - entry, exit, and survival - from the same
676 initial population of dauers in conditions similar to their ecology. In its natural environment,
677 *Pristionchus* is found primarily as dauers in soil and on its invertebrate hosts, predominantly
678 beetles [20,30]. The ability to enter dauer is vital to ensure success in the wild, as diminishing
679 food resources are a common occurrence. Worms that do not enter dauer under unfavorable
680 conditions risk preserving their populations. In addition to persevering through
681 unpredictable food availability, *Pristionchus* faces interspecific competition [67,68]. The
682 speed of dauer exit may determine the success of a population if cohabitating with another
683 nematode species, as first to the feast may establish, repopulate, and consume all accessible
684 bacteria [68]. Long-term survival in dauer provides protection during extended periods of
685 stressful conditions [30], and may play a role in evading competition while waiting for
686 microbial populations to reestablish [68].
687 Therefore, starvation resistance is a trait that is crucial for the fitness of these worms
688 in the wild: adults need to adjust to starvation and invest into the production of viable eggs,
689 allowing future generations of worms to persist; dauers need to be able to survive over

690 extended periods of time, allowing them to disperse and establish new populations of
691 reproducing worms under suitable conditions. Here, we demonstrated that the
692 supplementary nuclear receptor *Ppa*-NHR-10 contributes to the transcriptional regulation
693 of starvation responses in *P. pacificus*, and that it is required for starvation resistance in
694 adults and dauer larvae. Based on our transcriptomic experiments and our survival data,
695 we propose that the underlying mechanism through which this is achieved is based on the
696 activation and β-oxidation of fatty acids. Future molecular genetic investigations will be able
697 to directly test this hypothesis based on the candidate targets we identified in our
698 experiments, ultimately expanding our understanding of the physiological and genetic
699 mechanisms that underlie starvation resistance in these nematodes.
700

Material & methods

Nematode husbandry

We followed standard protocols for the establishment and maintenance of laboratory cultures of rhabditid and diplogastrid nematodes [65]. Briefly, nematodes of all strains used in this study were cultured on nematode growth medium (NGM) in 6cm Petri dishes, using the uracil-auxotrophic strain "OP50" of *Escherichia coli* as a food source. Bacteria were grown overnight at 37°C in LB medium. We generally added 300μl of fresh bacterial food solution to each Petri dish and left these plates at room temperature for several days, in order to allow the bacterial lawns to grow. Usually, five gravid adult hermaphrodites were transferred to these fresh plates to maintain cultures. Culture plates were stored in plastic boxes and kept in an incubator set to a constant 20°C.

Light microscopy with differential interference contrast (DIC) and morph ratios

For microscopy, all specimens were mounted on object slides with 5% Noble Agar pads which contained the sedative sodium azide (0.5% NaN_3) and subsequently examined using a Zeiss Axio Imager.Z1 microscope with a Zeiss Plan-Apochromate 100 x 1.4 DIC objective. Image stacks (Grayscale, 16-bit) were taken using a monochromatic Zeiss Axiocam 506 CCD camera. The Zen 2 Pro Software (Carl Zeiss Microscopy GmbH, 2011; version 2.0.14283.302; 64-bit) for digital microscopic analysis and image acquisition.

Relative ratios of eurystomaous (Eu) and stenostomatous (St) morphologies in each strain were scored using the aforementioned microscopy settings. Worms that had a large right ventrosublateral tooth, a hook-shaped dorsal tooth, and a promesostegostom whose anterior tips were clearly posterior to those of the gymnostom were classified as Eu morphs; animals that did not meet these combined characteristics were scored as St morphs. Statistical differences in morph ratios were assessed via a PERMANOVA (see "Dauer assays" section of the methods for details).

Quantification of morphological differences in mutant animals

We quantified morphological differences in the mouths of wild-type and mutant worms, using our recently published protocol [69]. This approach combines 2-dimensional landmark-based geometric morphometrics (GMM) with unsupervised clustering methods.

For this study, we obtained image stacks of the nematode mouths in lateral position and recorded the X and Y coordinates of 18 fixed landmarks which capture the overall form of the mouth using FIJI (ver. 2.1.0) [70]. All steps of the GMM analysis were performed in R (ver. 4.3.0) [71] using a combination of the GEOMORPH (ver. 4.0.5) [72-74], MORPHO (ver. 2.11) [40,41], and MCLUST (ver. 6.0.0.) packages [75,76]. General Procrustes Analysis (GPA) was performed with the *gpagen* function of GEOMORPH, by minimizing Procrustes distances. Procrustes coordinates were projected into a linear tangent space in order to obtain Euclidean distances for downstream statistical analysis. We originally generated landmark data for 150 animals (50 per strain; three strains: PS312, RS3920, RS3921), performed a GPA and subsequently checked for Procrustes distance outliers in our original shape data. Outliers were identified separately for each of the strains of interest, using the *plotOutliers* function of GEOMORPH. Six extreme outliers were identified and removed from the original data to facilitate downstream analysis. The outlier-corrected data set (n=144) thus contained landmark configurations of 48 animals per strain. This dataset was used to quantify

differences in mouth form and to see whether mutant animals can be classified as such, based on the structure of their mouths. In morphometric terms, form refers to all morphological variation in the data, i.e. the variation in both shape and size [77]. As form data takes into account the full spectrum of structural variation between the groups of interest, it generally outperforms pure shape or size datasets for classification tasks such as ours [78].

We generated form data by first performing a GPA on our outlier-corrected landmark dataset to obtain a shape matrix to which subsequently appended a size variable (here, the log-transformed centroid size). We performed a principal component analysis (PCA) on the form data to visualize potential morphological differences among wild-type and mutant worms in a form space *sensu* Mitteroecker *et al.* [79]. We tested whether the form data contains clearly separable groups of specimens with similar morphology, ideally ones which correspond to the different strains. For this, we performed model-based clustering with the *Mclust* function of the MCLUST package. We only used "meaningful" principal components (mPCs) of form variation (identified with MORPHO's *getMeaningfulPCs* function [40,41]) as input variables for unsupervised clustering, in order to avoid overparameterization of our multivariate normal models [69]. Finally, we visualized the clustering results in the form space (i.e., the form PCA plot) by coloring each specimen according to the identified cluster to which it belongs.

CRISPR/CAS9 mutagenesis

We used the CRISPR/CAS9 system to create small "indel" mutations in the coding sequences of *Ppa-nhr-10*, specifically in the part of the gene that encodes the ligand-binding domain (LBD) of *Ppa*-NHR-10. For this we followed established mutagenesis protocols for model nematodes [80,81]. Target-specific CRISPR RNAs (crRNAs) were generated based on the publicly available genome sequence of *P. pacificus* (www.pristionchus.org; El Paco ver. 3) and designed to target 20bp upstream of a 5'-NGG-3'-protospacer adjacent motif (PAM). The CAS9 protein (cat.nr.: 1081058; IDT), the universal trans-acting CRISPR RNA (tracrRNA), and all crRNAs were ordered from IDT (Alt-R product line). Ribonucleoprotein complexes (RNPs) were created by combining 0.5μl of CAS9 nuclease (10μg/ml stock) with 5μl of tracrRNA (0.4μg/μl stock) and 2.8μl of crRNA (0.4μg/μl stock). This mix was incubated at 37°C for 15min and subsequently cooled down to room temperature. The RNP mix was diluted by adding enough Tris-EDTA buffer to bing the total volume of the injection mix to 20μl. In order to avoid clogging in the injection needles, the final mix was centrifuged at 14,000rpm for 2min. Injections were conducted with an Eppendorf FemtoJet microinjector at 400x magnification under an inverse Zeiss AxioVert microscope that was equipped with a Zeiss Plan-Apochromat 40x DIC objective and coupled to an Eppendorf TransferMan micromanipulator. Injections were aimed at the distal tip of the hermaphrodite gonad in young adults; animals were punctured in a 45° angle to the anterior-posterior body axis and RNP complexes were injected into the gonadal rachis. Injected P0 animals were isolated onto separate NGM plates and allowed to lay eggs for 24h at 20°C. After that, P0s were removed from the plates and F1 animals were left to grow. Upon reaching maturity, F1s were singled out to fresh plates, allowed to lay eggs for 24h and subsequently used for genotyping. DNA of candidate F1 animals was recovered via single worm lysis (SWL). In short, individual worms were placed in 10μl of SWL buffer (10mM Tris-HCl at pH=8.3, 50mM KCl, 2.5mM $MgCl_2$, 0.45% NP-40, 0.45% Tween 20, 120μg/ml Proteinase K) and frozen at -80°C for 20min. Afterwards, all samples were

794 incubated in a thermocycler at 65°C for 1h, followed by a heat inactivation of the proteinase
795 at 95°C for 10min. This lysate was used as a template for subsequent PCR amplification
796 (using the Taq PCR Master Mix produced by Qiagen) of the region of interest. Potential
797 mutations in candidate amplicons were identified using Sanger sequencing. Sanger
798 sequencing was performed by Azenta Life Sciences. If heterozygous F1 mutants were found,
799 their F2 offspring were genotyped in a similar fashion, to identify homozygous mutant
800 carriers. Multiple homozygous mutant lines were isolated, including frameshift mutants
801 with premature stop codons. Backups of the original homozygous mutant strains were
802 frozen and stored at -80°C.
803

804 **Transgenesis**

805 To visualize which cells actively express *Ppa-nhr-10*, we generated transcriptional reporter
806 lines. We PCR-amplified a 1.371 bp long putative promoter sequence, starting right before
807 the start codon of *Ppa-nhr-10*, and subsequently cloned it into a pUC19 vector that contained
808 a codon-optimized GFP with *P. pacificus* introns and the *Ppa-rpl-23* 3'UTR [82]. We generally
809 used the NEBuilder HiFi DNA Assembly Kit for Gibson assemblies, *E. coli* (NEB 5-alpha)
810 for bacterial transformation, and InVitrogen's PureLink HQ Mini Plasmid kit (including the
811 optional, but essential, wash step with PB buffer) for plasmid extraction from 3ml bacterial
812 overnight cultures. The *Ppa-nhr-10p::GFP* construct was linearized with SphI-HF (New
813 England BioLabs) according to manufacturer's instructions. Following established
814 protocols, we combined 10 ng/μl of our linearized plasmid were injected into the gonad of
815 the wild-type strain of *P. pacificus* (PS312), together with 60 ng/μl of SphI-linearized
816 genomic carrier DNA and 10 ng/μl of SphI-linearized co-injection marker *Ppa-egl-20p::RFP*
817 [82,83]. We confirmed that expression patterns were consistent across two independent
818 reporter lines (Fig 2A and 2B). Fluorescent worms were imaged using a Leica SP8 confocal
819 laser-scanning microscope (cLSM).
820

821 **Exploratory RNA-seq experiments - sequencing mutant larvae and adults**

822 To facilitate *exploratory* RNA-seq analysis on our *Ppa-nhr-10* mutants comparable to
823 the RNA-seq experiments our lab previously conducted on *Ppa-nhr-1* and *Ppa-nhr-40*
824 mutants, we adopted (with minor modifications) the sample collection and sequencing
825 approaches that were used by Sieriebriennikov *et al.* [24]. We first transferred seven gravid
826 adult *P. pacificus* hermaphrodites to fresh agar plates that were spotted with 300μl of OP50
827 *E. coli*. These worms were kept at 20°C for 4-5 days, in order to obtain sufficient starting
828 amounts of eggs (F2) laid by their F1 offspring. To isolate the eggs, we suspended all worms
829 and eggs on an individual plate in 1ml water, collected such suspensions form multiple
830 plates in 15ml Falcon tubes, and incubated these samples for 10min in a mix of 0.5M NaOH
831 and household bleach (1:5 dilution). The Falcon tubes were vortexed every other minute to
832 disintegrate the post-hatching life stages. The eggs were centrifuge-pelleted at 500g for
833 2min, resuspended in 5ml water, and pelleted again; this washing process was repeated
834 three times. In the final step, we resuspended the egg pellets in 1ml water and subsequently
835 pipetted 100μl onto fresh agar plates that were kept at 20°C. Animals were collected for
836 RNA extraction at 24h (mostly J2 and a few J3 larvae), 50h (J3 and J4 larvae), and 70h (young
837 adults) after bleaching; the presence and expected distribution of the desired stages at each
838 time point was verified prior to sample collection by screening 50 specimens on each plate
839 under a dissecting microscope. Worms were collected by adding 1ml water to each of the
840 plates, scraping off the bacterial lawns containing the animals with Lazy L-shaped

841 spreaders, filtering the worms out of the resulting suspension with a 5μm nylon net filter,
842 and washing the animals off the filters into 1.5ml Eppendorf tubes with water. Finally, the
843 eggs were pelleted in these tubes at maximum speed for 2min using a tabletop centrifugate,
844 and the supernatant was discarded. Total RNA was extracted using the Direct-Zol RNA
845 Mini prep kit (Zymo Research) according to the instructions provided by the manufacturer.
846 Following Sieriebriennikov *et al.*'s approach [24], we combined 500ng of RNA that was
847 extracted at the 24h time point with 500ng of RNA extracted at the 50h time point. This
848 sample type thus contains a total of 1μg RNA extracted from J2-4 larvae. On the other hand,
849 we gathered 1μg of RNA extracted at the 70h time point (adult worms) and did not mix it
850 with RNA extracted from any other time point. Therefore, we ended up with two sample
851 types (for simplicity referred to as "larval" and "adult"), which we shipped to Novogene for
852 library preparation and mRNA sequencing. Libraries were sequenced as 150bp paired end
853 reads on Illumina's NovaSeq6000 platform. We sequenced the mRNA of three strains: the
854 wild-type *P. pacificus* strain (PS312), and two independently acquired frameshift mutants of
855 *Ppa-nhr-10* (RS3920 and RS3921). Two biological replicates were collected for the larval and
856 adult stages of each of these three strains.
857
858 **Confirmatory RNA-seq experiments - sequencing starving worms**
859 We also performed *confirmatory* RNA-seq experiments, in order to properly identify
860 *Ppa*-NHR-10's regulatory targets in the same conditions in which we identified the survival
861 phenotype of mutant animals. Additionally, we aimed to investigate the wild-type
862 starvation response of *P. pacificus*. Therefore, using our starvation assay set-up (see
863 "Starvation assays and survival analysis"), we sequenced mRNA extracted from young
864 adult hermaphrodites which have been well-fed or acutely-starved for 24 hours (in liquid
865 cultures). Just like for the exploratory RNA-seq experiments, we used the wild-type strain
866 (PS312) of *P. pacificus* and the two reference *Ppa-nhr-10(lof)* strains (RS3920 and RS3921) for
867 these confirmatory RNA-seq experiments. After the liquid culture treatments, we generally
868 washed the worms three times with 0.5% Triton X-100/PBS and three times with PBS
869 through a 20μm nylon filter net, and subsequently preformed total-RNA extractions with
870 the Direct-Zol RNA Mini prep kit (Zymo Research), following manufacturer instructions.
871 For each sample, ~1μg of total RNA was extracted and shipped to Novogene for library
872 preparation and mRNA sequencing. As before, libraries were sequenced as 150bp paired
873 end reads on Illumina's NovaSeq6000 platform. This time, we sequenced three biological
874 replicates for each the three strains in each of the two conditions.
875
876 **Quantification of transcripts and differential expression analysis (DEA)**
877 Transcript abundances were estimated from the obtained raw read files relative to the *P.*
878 *pacificus* transcriptome using SALMON (ver. 1.5.2) [84,85]. We first build a decoy-aware
879 transcriptome file, using the entire *P. pacificus* genome as a decoy, following the exact
880 instructions of Salmon's online documentation (see
881 https://salmon.readthedocs.io/en/latest/salmon.html under "Preparing transcriptome
882 indices (mapping-based mode)"). The decoy-aware transcriptome was then indexed for
883 subsequent read-mapping using an auxiliary *k*-mer hash over *k*-mers of the length of 31.
884 Reads were quantified directly against this index using Salmon's *quant* command, by
885 running the program in mapping-based mode with selective alignment as mapping strategy
886 ("--validateMappings" flag). We allowed Salmon to automatically infer the library type ("-l

887 A" flag), and to simultaneously learn and correct for fragment-level GC-biases and
888 sequence-specific biases ("-- gcBias" and "-- seqBias" flags).
889 Differential expression analyses were carried out in R using BIOCONDUCTOR (ver.
890 3.17) [86], TXIMPORT (ver. 1.28.0) [87], and DESEQ2 (ver. 1.40.1) [49]. First, we created a
891 "transcript-name to gene-ID" cross-reference map ("tx2gene") from the publicly available *P.*
892 *pacificus* gene annotations using the GENOMICFEATURES (ver. 1.48.3) [88] and
893 ANNOTATIONDBI (ver. 1.58.0) [89] packages. After that, we summarized the transcript-level
894 abundance estimates generated by Salmon into gene-level count matrices using the *tximport*
895 function together with our tx2gene map. The *DESeqDataSetFromTximport* function of
896 DESEQ2 was used to specify the statistical designs for the analyses and the dataset was pre-
897 filtered for transcripts which had at least ten counts across all samples. We generally
898 performed multifactorial DEA by first combining the two factors of interest (i.e., "stage" and
899 "strain" in the exploratory RNA-seq experiments; or "condition" and "strain" in confirmatory
900 RNA-seq) into a single factor called "group" and subsequently modeled the mutation-effects
901 on transcript abundances in each stage or condition (e.g. "RS3920_larvae" *vs.*
902 "wildtype_larvae", or "RS3920_starved" *vs.* "wildtype_starved") using the *DESeq* function
903 [86]. The same logic was followed to extract the effect of starvation on wild-type worms (i.e.,
904 "wildtype_starved" *vs.* "wildtype_fed").
905 The obtained maximum likelihood estimates (MLE) of the log2-fold changes (L2FC)
906 for each gene were shrunken with the *lfcShrink* function using the adaptive shrinkage
907 estimator from the ASHR package [90]. This approach fits a mixture of normal distributions
908 to form an empirical Bayesian prior for the shrinkage procedure, in order to overcome the
909 strong heteroskedasticity in L2FC-estimates for genes with low counts while
910 simultaneously avoiding over-shrinkage of large L2FC-estimates [49]. The resulting
911 (shrunken) minimum mean squared error (MMSE) estimates of the L2FC were reported for
912 this study and used to rank and visualize candidate target genes.
913 Additionally, following recent advancements in the field of genomics, we abstained
914 from using the classical hypothesis testing approach for DEA, which assumes a "L2FC = 0"
915 as the null hypothesis and calculates FDR-corrected *P*-values (aka *q*-values) to claim
916 discoveries [49]. Briefly, this classical approach computes *P*-values, which tell us only how
917 confident we can be that there is any observable effect. These *P*-values, unfortunately, do
918 not at all tell us how confident we can be in either the estimated size of the effect or its
919 estimated direction. This problem can be addressed by hypothesis tests that (I) include a
920 minimum effect size in the null hypothesis (e.g. L2FC ≥ 'x'), and (II) compute *s*-values. In
921 this approach, the *s*-values report what we are actually interested in: whether the evidence
922 in the data is strong enough to support the belief that an effect can be observed, that the
923 observed effect is at least of the specified minimum size 'x', and that the direction of the
924 effect was correctly estimated [49,90]. For this reason, in order to infer differentially
925 expressed genes from our transcriptome data, we always included a L2FC-threshold of >
926 0.585 (absolute value) and a *s*-value threshold of < 0.005 into our hypothesis tests. This is
927 equivalent to asking, whether there is sufficient evidence in the data that a given gene is
928 indeed differentially expressed, that it is at least 50% up- or down-regulated, and that the
929 direction of this effect (up *vs.* down) was correctly estimated.
930
931 **Starvation assays and survival analysis**
932 Young adult hermaphrodites (day one of adulthood) were washed off of multiple agar
933 plates with 0.5% Triton-X100/PBS and a lazy-L scraper. The collected worm solutions were

934 filtered through a 20 μm nylon net filter and washed three times with 1ml 0.5% Triton-
935 X100/PBS and, subsequently, three times with 1ml PBS. The bacteria-free worm pellets were
936 resuspended in 250μl S-medium without cholesterol and added to empty agarose plates.
937 The S-medium was allowed to be absorbed by the agarose and the clean worms were
938 allowed to recover for one hour. During the recovery time, liquid cultures were set up for
939 the experiments. We used small cell culture flasks (50ml) for our assays and added a total
940 amount of 2.5ml liquid culture (LC) to each of them. The LCs for the acute starvation assays
941 consisted only of 2.5ml S-medium (without cholesterol). The control LC with plenty of food
942 were set up as follows: for each 2.5ml of final LC, we centrifuged 10ml of fresh bacterial
943 stock solution (*E. coli* OP50, OD_{600} = 0.5) for 30min at 4250rpm (4°C). The bacterial pellets
944 were resuspended in the according amount (2.5ml per assay flask) of S-medium without
945 liquid culture and added to the cell culture flasks. To prevent unwanted microbial
946 contaminations, we added 1μl of nystatin and 1.2μl of streptomycin to each assay flask,
947 irrespective of whether it contained OP50 or not. Finally, we picked the young
948 hermaphrodites which recovered from the washing step and added them to the assay flasks
949 (~50 worms per flask). All assay flasks were kept in a shaking incubator set to 20°C and
950 130rpm and the ratio of alive worms was scored every 24hrs until all worms in the flask
951 were dead. Media were replaced every third day in order to limit bacterial contaminations
952 and remove offspring animals produced in the well-fed conditions. Overall differences in
953 the survival curves within each of the two treatments were estimated using the Kaplan-
954 Meier (KM) approach [91]. Pairwise comparisons among individual survival curves were
955 based on the KM estimator and performed using the log-rank test [90]. Additionally, we
956 estimated hazard rates for each of the strains in both experiments via Cox proportional
957 hazard regression modeling [91,92]. Effect sizes were calculated as hazard ratios which
958 compare the hazard rates of *Ppa-nhr-10(lof)* mutants (RS3920 and RS3921) to the wild-type
959 hazard rate. *P*-values were corrected for false discoveries using the Bonferroni method. All
960 survival analyses were carried out in R (ver. 4.3.0) [71] using the SURVIVAL (ver. 3.5-5),
961 GGSURVFIT (ver. 0.3.0), SURVMINER (ver. 0.4.9), and GTSUMMARY (ver. 1.7.1) packages [93-96].
962 All survival experiments were repeated four times (N=4) independently with all three
963 strains.
964

965 **Phylogram of the NHR-1/-10/-40 cluster**

966 We searched the genomes of ten nematode species for orthologs of *Ppa*-NHR-1, *Ppa*-NHR-
967 10, and *Ppa*-NHR-40, using BLASTP ($e < 0.0001$). The list of genomes included *Brugia malayi*
968 (clade III - Spiruromorpha), *Bursaphelenchus xylophilus* (clade IV - Tylenchida), *Panagrellus*
969 *redivivus* (clade IV - Tylenchida), *Oscheius tipulae* (clade V - Rhabditida), *Caenorhabditis*
970 *briggsae* (clade V - Rhabditida), *Caenorhabditis elegans* (clade V - Rhabditida; wormbase.org
971 WS289), *Haemonchus contortus* (clade V - Strongylida), *Micoletzkya japonica* (clade V -
972 Diplogasterida), *Parapristionchus giblindavisi* (clade V - Diplogasterida), and *Pristionchus*
973 *pacificus* (clade V - Diplogasterida) [97-106] (non-diplogastrids: WormBase ParaSite ver.
974 WBPS18; diplogastrids: pristionchus.org). The protein sequences of the obtained orthologs
975 were aligned with MAFFT (ver. 7.48) using default settings [107]. Based on the results of the
976 multiple sequence alignments, we calculated maximum likelihood trees in R (ver. 4.3.0) [71]
977 using the PHANGORN (ver. 2.11.1) package [108] applying a LG substitution model with
978 optimization of topology and base frequencies over 100 bootstrap replicates.
979

980 **Pfam domain prediction, WormCat annotation, and overrepresentation analyses**

Protein domains encoded in the proteome of *P. pacificus* were predicted using HMMER (ver. 3.3.2) [109] in conjunction with the Pfam-A.hmm database (ver. 3.1b2) [47] (hmmscan, e-value cutoff: < 0.001). The ORTHOFINDER software (default mode; ver. 2.5.4) [110] was used to define orthogroups of *P. pacificus* and *C. elegans* proteins; WormCat (ver. 2) annotations [48] for *P. pacificus* were created based on the obtained orthogroups. In a few cases, we found multiple *C. elegans* orthologs with different WormCat terms for an individual *P. pacificus* gene. In such cases, we transferred all unique WormCat terms among the orthologs to the given gene in *P. pacificus*. All overrepresentation analyses (ORAs) were based on Fisher's Exact test; obtained *P*-values were FDR-corrected.

Dauer assays

We performed three different assays regarding dauer biology: dauer entry, dauer exit, and dauer survival. The workflow of these assays is depicted in Fig 8A. First, we added a starting population of 500 young adult worms to 10ml standard liquid cultures (LCs) with OP50 as a food source (S-medium with or without cholesterol, 4μl nystatin and 5μl Streptomycin added). Worms were allowed to propagated for two weeks at 22°C and 180rpm. After two weeks we extracted 10μl from each LC and counted the number of dauers versus the number of feeding stages in the sample to quantify dauer entry (in %). The remaining volume of the LCs was treated with SDS following standard protocols [111] to isolate dauers. Some of the obtained dauers were added to agarose plates spotted with 300μl OP50 (30 worms per plate) and followed for multiple days to quantify the speed of dauer exit. These plates were kept at 20°C and worms were scored every 24 hrs until every individual exited the dauer arrest. The rest of the SDS-isolated dauers was added to LCs for the survival assays. These LCs did not contain food nor cholesterol and were again kept at 22°C and 180rpm for up to three weeks. Every week, we extracted 75μl of worm solution and added 25μl to three OP50-spotted agarose plates. We let the worms recover on these plates for 24 hrs and then scored alive versus dead worms to obtain the ratio of survivors (in %). All experiments were repeated multiple times independently (N=4). For the dauer exit and dauer survival assays we exclusively used dauers isolated from LCs that did not contain cholesterol. To statistically assess whether there are mutant-specific phenotypes in dauer entry, dauer exit, or dauer survival, we applied a two-tailed PERMANOVA [112,113] with null model residual randomization (RRPP) using the *lm.rrpp* function of the RRPP package (ver. 1.3.1) [114,115]. Relative effect sizes (Z-scores) and *P*-values are reported in Fig 8B-8D. We considered our dauer data as incompatible with the null hypothesis (i.e., "statistically significant") if the relative effect size was at least twice as large as the standard deviation ($Z \geq 2.0$) and the *P*-value was below a type I error rate of 5% ($P < 0.05$). If at least one of these criteria was not met, we considered the data compatible with the null hypothesis (i.e., "not statistically significant"). Null model residuals were randomized and permuted 10,000 times. Pairwise comparisons of mutant and wild-type strains were performed with the *pairwise* function of RRPP [114,115].

Data processing, data visualization, and illustration

All data was processed, formatted, and wrangled in R (ver. 4.3.0) [71] using the TIDYVERSE [116]. All scientific plots depicted in this study were created using the GGPLOT2 package (ver. 3.4.2) [116]. Heatmaps were created using the PHEATMAP package (ver. 1.0.12) [117]. In order to make our plots accessible to people with color-vision deficiencies or color blindness [118], we exclusively used the scientifically-derived colormaps provided by the SCICO (ver. 1.4.0)

[119] and VIRIDIS (ver. 0.6.3) packages [120]. Microscopic images were edited and adjusted for levels, lightness, and contrast, in Affinity Photo (1.10.5). Scientific illustrations and final figures were created in Affinity Designer (ver. 1.10.5).

Author contributions

Conceptualization: Tobias Theska.
Data curation: Tobias Theska.
Formal analysis: Tobias Theska.
Funding acquisition: Ralf J. Sommer.
Investigation: Tobias Theska, Tess Renahan.
Methodology: Tobias Theska, Tess Renahan.
Project administration: Tobias Theska.
Resources: Ralf J. Sommer.
Software: Tobias Theska.
Supervision: Ralf J. Sommer.
Validation: Tobias Theska, Tess Renahan.
Visualization: Tobias Theska.
Writing - original draft: Tobias Theska.
Writing - review & editing: Tobias Theska, Tess Renahan, Ralf J. Sommer.

Competing interests

The authors declare no competing interests.

Data availability statement

Raw reads from the mRNA-seq experiments have been deposited in the European Nucleotide Archive (ENA) under the accession number PRJEB65081. Primer information, morph ratio data, landmark data for geometric morphometrics, Kaplan-Meier starvation survival data, differential expression analysis results, and dauer assay data are provided in the supplementary material (Sup Data 1-10).

Acknowledgements

We thank the Light Microscopy facility at the Max Planck Institute for Biology, especially Christian Feldhaus and Aurora Panzera, for their assistance with confocal laser-scanning microscopy. We are grateful to Heike Haussmann for freezing samples of all the worm strains produced for this study. Additionally, we thank Christian Rödelsperger, Adrian Streit, and Devansh R. Sharma for helpful discussions of our work.

References

1. Van Den Hoogen J, Geisen S, Routh D, Ferris H, Traunspurger W, Wardle DA, et al. Soil nematode abundance and functional group composition at a global scale. Nature. 2019;572:194–198.
2. Lambshead PJD, Boucher G. Marine nematode deep-sea biodiversity–hyperdiverse or hype? Journal of Biogeography. 2003;30:475–485.
3. Blaxter M. Nematodes: the worm and its relatives. PLOS Biology. 2011;9:e1001050.
4. Corsi AK, Wightman B, Chalfie M. A transparent window into biology: a primer on *Caenorhabditis elegans*. Genetics. 2015;200:387–407.
5. Watts JL, Ristow M. Lipid and carbohydrate metabolism in *Caenorhabditis elegans*. Genetics. 2017;207:413–446.
6. Baugh LR, Hu PJ. Starvation responses throughout the *Caenorhabditis elegans* life cycle. Genetics. 2020;216:837–878.
7. Rothman J, Jarriault S. Developmental plasticity and cellular reprogramming in *Caenorhabditis elegans*. Genetics. 2019;213:723–757.
8. Conradt B, Wu YC, Xue D. Programmed cell death during *Caenorhabditis elegans* development. Genetics. 2016;203:1533–1562.
9. Moss EG. Heterochronic genes and the nature of developmental time. Current Biology. 2007;17:R425–434.
10. Sommer RJ. Evolution of regulatory networks: nematode vulva induction as an example of developmental systems drift. In: Soyer O, editors. Evolutionary Systems Biology. Springer; 2012. p. 79–91.
11. Viney M, Diaz A. Phenotypic plasticity in nematodes: evolutionary and ecological significance. Worm. 2012; 1:98–106.
12. Sommer RJ, Dardiry M, Lenuzzi M, Namdeo S, Renahan T, Sieriebriennikov B, et al. The genetics of phenotypic plasticity in nematode feeding structures. Open biology. 2017;7:160332.
13. Sommer RJ, Ogawa A. Hormone signaling and phenotypic plasticity in nematode development and evolution. Current Biology. 2011;21:R758–766.
14. Haag ES, Fitch DH, Delattre M. From "the worm" to "the worms" and back again: the evolutionary developmental biology of nematodes. Genetics. 2018;210:397–433.
15. West-Eberhard MJ. Developmental plasticity and evolution. Oxford; New York: Oxford University Press; 2003.
16. Laland KN, Uller T, Feldman MW, Sterelny K, Müller GB, Moczek A, et al. The extended evolutionary synthesis: its structure, assumptions and predictions. Proceedings of the Royal Society B: Biological Sciences. 2015;282:20151019.
17. Uller T, Feiner N, Radersma R, Jackson IS, Rago A. Developmental plasticity and evolutionary explanations. Evolution & Development. 2020;22:47–55.
18. Sommer RJ. Phenotypic plasticity: from theory and genetics to current and future challenges. Genetics. 2020;215:1–13.
19. Hong RL, Sommer RJ. *Pristionchus pacificus*: a well-rounded nematode. Bioessays. 2006;28:651–659.
20. Sommer RJ. *Pristionchus pacificus*: a nematode model for comparative and evolutionary biology. Vol. 11. Leiden; The Netherlands: Brill; 2015.
21. Ragsdale EJ, Müller MR, Rödelsperger C, Sommer RJ. A developmental switch coupled to the evolution of plasticity acts through a sulfatase. Cell. 2013;155:922–933.
22. Kieninger MR, Ivers NA, Rödelsperger C, Markov GV, Sommer RJ, Ragsdale EJ. The nuclear hormone receptor NHR-40 acts downstream of the sulfatase EUD-1 as part of a developmental plasticity switch in *Pristionchus*. Current Biology. 2016;26:2174–2179.
23. Sieriebriennikov B, Prabh N, Dardiry M, Witte H, Röseler W, Kieninger MR, et al. A developmental switch generating phenotypic plasticity is part of a conserved multi-gene locus. Cell Reports. 2018;23:2835–2843.

24. Sieriebriennikov B, Sun S, Lightfoot JW, Witte H, Moreno E, Rödelsperger C, et al. Conserved nuclear hormone receptors controlling a novel plastic trait target fast-evolving genes expressed in a single cell. PLOS Genetics. 2020;16:e1008687.

25. Sun S, Theska T, Witte H, Ragsdale EJ, Sommer RJ. The oscillating Mucin-type protein DPY-6 has a conserved role in nematode mouth and cuticle formation. Genetics. 2022;220:iyab233.

26. Sun S, Witte H, Sommer RJ. Chitin contributes to the formation of a feeding structure in a predatory nematode. Current Biology. 2023;33:15–27.

27. Werner MS, Loschko T, King T, Reich S, Theska T, Franz-Wachtel M, et al. Histone 4 lysine 5/12 acetylation enables developmental plasticity of *Pristionchus* mouth form. Nature Communications. 2023;14:2095.

28. Cassada RC, Russell RL. The dauerlarva, a post-embryonic developmental variant of the nematode *Caenorhabditis elegans*. Developmental biology. 1975;46:326–342.

29. Ogawa A, Streit A, Antebi A, Sommer RJ. A conserved endocrine mechanism controls the formation of dauer and infective larvae in nematodes. Current Biology. 2009;19:67–71.

30. Renahan T, Lo W, Werner MS, Rochat J, Herrmann M, Sommer RJ. Nematode biphasic 'boom and bust' dynamics are dependent on host bacterial load while linking dauer and mouth-form polyphenisms. Environmental Microbiology. 2021;23:5102–5113.

31. Motola DL, Cummins CL, Rottiers V, Sharma KK, Li T, Li Y, et al. Identification of ligands for DAF-12 that govern dauer formation and reproduction in *C. elegans*. Cell. 2006;124:1209–1223.

32. Tao LJ, Seo DE, Jackson B, Ivanova NB, Santori FR. Nuclear hormone receptors and their ligands: metabolites in control of transcription. Cells. 2020;9:2606.

33. Miglioli A, Canesi L, Gomes ID, Schubert M, Dumollard R. Nuclear receptors and development of marine invertebrates. Genes. 2021;12:83.

34. Sural S, Hobert O. Nematode nuclear receptors as integrators of sensory information. Current Biology. 2021;31:4361–4366.

35. Sluder AE, Mathews SW, Hough D, Yin VP, Maina CV. The nuclear receptor superfamily has undergone extensive proliferation and diversification in nematodes. Genome Research. 1999;9:103–120.

36. Robinson-Rechavi M, Maina CV, Gissendanner CR, Laudet V, Sluder A. Explosive lineage-specific expansion of the orphan nuclear receptor HNF4 in nematodes. Journal of Molecular Evolution. 2005;60:577–586.

37. Peterson ND, Samantha YT, Huang QJ, Wani KA, Schiffer CA, Pukkila-Worley R. Non-canonical pattern recognition of a pathogen-derived metabolite by a nuclear hormone receptor identifies virulent bacteria in *C. elegans*. Immunity. 2023;56:768–782.

38. Howard RJ, Giacomelli M, Lozano-Fernandez J, Edgecombe GD, Fleming JF, Kristensen RM, et al. The Ediacaran origin of Ecdysozoa: integrating fossil and phylogenomic data. Journal of the Geological Society. 2022;179(4):jgs2021-107.

39. Riebesell M, Sommer RJ. Three-dimensional reconstruction of the pharyngeal gland cells in the predatory nematode *Pristionchus pacificus*. Journal of Morphology. 2017;278:1656–1666.

40. Schlager S. Morpho and Rvcg–Shape Analysis in R: R-Packages for geometric morphometrics, shape analysis and surface manipulations. In: Zheng G, Li S, Szekely G, editors. Statistical Shape and Deformation Analysis. Academic Press; 2017. p. 217–256.

41. Schlager S, Jefferis G. Morpho: calculations and visualisations related to geometric morphometrics. R package version 2.11. 2023. Available from: https://cran.r-project.org/web/packages/Morpho/index.html

42. Hu PJ. Dauer. In: The *C. elegans* research community, editor. WormBook: The Online Review of *C. elegans* Biology. 2007.

43. Srinivasan S. Regulation of body fat in *Caenorhabditis elegans*. Annual Review of Physiology. 2015;77:161–178.

44. Lemieux GA, Ashrafi K. Neural regulatory pathways of feeding and fat in *Caenorhabditis elegans*. Annual Review of Genetics. 2015;49:413–438.

45. Hansen M, Flatt T, Aguilaniu H. Reproduction, fat metabolism, and life span: what is the connection? Cell Metabolism. 2013;17:10–19.

46. Athanasouli M, Akduman N, Röseler W, Theam P, Rödelsperger C. Thousands of *Pristionchus pacificus* orphan genes were integrated into developmental networks that respond to diverse environmental microbiota. PLOS Genetics. 2023;19:e1010832.

47. Finn RD, Coggill P, Eberhardt RY, Eddy SR, Mistry J, Mitchell AL, et al. The Pfam protein families database: towards a more sustainable future. Nucleic Acids Research. 2016;44:D279–285.

48. Holdorf AD, Higgins DP, Hart AC, Boag PR, Pazour GJ, Walhout AJ, et al. WormCat: an online tool for annotation and visualization of *Caenorhabditis elegans* genome-scale data. Genetics. 2020;214:279–294.

49. Love MI, Huber W, Anders S. Moderated estimation of fold change and dispersion for RNA-seq data with DESeq2. Genome Biology. 2014;15:1–21.

50. O'Riordan VB, Burnell AM. Intermediary metabolism in the dauer larva of the nematode *Caenorhabditis elegans* II. The glyoxylate cycle and fatty-acid oxidation. Comparative Biochemistry and Physiology B, Comparative Biochemistry. 1990;95:125–130.

51. Braeckman B, Houthoofd K, Vanfleteren J. Intermediary metabolism. In: The *C. elegans* research community, editor. WormBook: The Online Review of *C. elegans* Biology. 2009.

52. Erkut C, Gade VR, Laxman S, Kurzchalia TV. The glyoxylate shunt is essential for desiccation tolerance in *C. elegans* and budding yeast. Elife. 2016;5:e13614.

53. Hibshman JD, Doan AE, Moore BT, Kaplan RE, Hung A, Webster AK, et al. daf-16/FoxO promotes gluconeogenesis and trehalose synthesis during starvation to support survival. Elife. 2017;6:e30057.

54. Abouheif E. Developmental genetics and homology: a hierarchical approach. Trends in Ecology & Evolution. 1997;12:405–408.

55. Amundson R. Form and Function in Evo-Devo. In: Nuño de la Rosa L, Müller GB, editors. Evolutionary Developmental Biology: A Reference Guide. Springer, Cham.; 2021, pp. 457–467.

56. Gabaldón T, Koonin EV. Functional and evolutionary implications of gene orthology. Nature Reviews Genetics. 2013;14:360–366.

57. Dolinski K, Botstein D. Orthology and functional conservation in eukaryotes. Annual Review of Genetics. 2007;41:465–507.

58. Nehrt NL, Clark WT, Radivojac P, Hahn MW. Testing the ortholog conjecture with comparative functional genomic data from mammals. PLOS Computational Biology. 2011;7:e1002073.

59. Dunn CW, Zapata F, Munro C, Siebert S, Hejnol A. Pairwise comparisons across species are problematic when analyzing functional genomic data. Proceedings of the National Academy of Sciences. 2018;115:E409–417.

60. Stamboulian M, Guerrero RF, Hahn MW, Radivojac P. The ortholog conjecture revisited: the value of orthologs and paralogs in function prediction. Bioinformatics. 2020;36:i219–i226.

61. Bulcha JT, Giese GE, Ali MZ, Lee YU, Walker MD, Holdorf AD, et al. A persistence detector for metabolic network rewiring in an animal. Cell Reports. 2019;26:460–468.

62. Stadler M, Fire A. Conserved translatome remodeling in nematode species executing a shared developmental transition. PLOS Genetics. 2013;9:e1003739.

63. Larance M, Pourkarimi E, Wang B, Murillo AB, Kent R, Lamond AI, et al. Global proteomics analysis of the response to starvation in *C. elegans*. Molecular & Cellular Proteomics. 2015;14:1989–2001.

64. Harvald EB, Sprenger RR, Dall KB, Ejsing CS, Nielsen R, Mandrup S, et al. Multi-omics analyses of starvation responses reveal a central role for lipoprotein metabolism in acute starvation survival in *C. elegans*. Cell Systems. 2017;5:38–52.

65. Stiernagle T. Maintenance of *C. elegans*. In: The *C. elegans* research community, editor. WormBook: The Online Review of *C. elegans* Biology. 2006.

66. Sanghvi GV, Baskaran P, Röseler W, Sieriebriennikov B, Rödelsperger C, Sommer RJ. Life history responses and gene expression profiles of the nematode *Pristionchus pacificus* cultured on *Cryptococcus* yeasts. PLOS One. 2016;11:e0164881.

67. Renahan T, Sommer RJ. Nematode interactions on beetle hosts indicate a role of mouth-form plasticity in resource competition. Frontiers in Ecology and Evolution. 2021;9:752695.

68. Renahan T, Sommer RJ. Multidimensional competition of nematodes affects plastic traits in a beetle ecosystem. Frontiers in Cell and Developmental Biology. 2022;10:985831.

69. Theska T, Sieriebriennikov B, Wighard SS, Werner MS, Sommer RJ. Geometric morphometrics of microscopic animals as exemplified by model nematodes. Nature Protocols. 2020;15:2611–2644.

70. Schindelin J, Arganda-Carreras I, Frise E, Kaynig V, Longair M, Pietzsch T, et al. Fiji: an open-source platform for biological-image analysis. Nature Methods. 2012;9:676–682.

71. R Core Team R. R: A language and environment for statistical computing. R Foundation for Statistical Computing. 2023.

72. Adams DC, Otárola-Castillo E. geomorph: an R package for the collection and analysis of geometric morphometric shape data. Methods in Ecology and Evolution. 2013;4:393–399.

73. Adams, D. C., Collyer, M. & Kaliontzopoulou, A. Geomorph: Software for geometric morphometric analyses. R package version 4.0.5. 2023. Available from: https://cran.r-project.org/web/packages/geomorph/index.html

74. Baken EK, Collyer ML, Kaliontzopoulou A, Adams DC. geomorph v4. 0 and gmShiny: Enhanced analytics and a new graphical interface for a comprehensive morphometric experience. Methods in Ecology and Evolution. 2021;12:2355–2363.

75. Scrucca L, Fop M, Murphy TB, Raftery AE. mclust 5: clustering, classification and density estimation using Gaussian finite mixture models. The R journal. 2016;8:289.

76. Fraley C, Raftery A, Scrucca L. mclust: Normal mixture modeling for model-based clustering, classification, and density estimation. R package version 6.0.0. 2023. Available from: https://cran.r-project.org/web/packages/mclust/index.html

77. Klingenberg CP. Size, shape, and form: concepts of allometry in geometric morphometrics. Development Genes and Evolution. 2016;226:113–137.

78. Mitteroecker P, Gunz P, Windhager S, Schaefer K. A brief review of shape, form, and allometry in geometric morphometrics, with applications to human facial morphology. Hystrix, the Italian Journal of Mammalogy. 2013;24:59–66.

79. Mitteroecker P, Gunz P, Bernhard M, Schaefer K, Bookstein FL. Comparison of cranial ontogenetic trajectories among great apes and humans. Journal of Human Evolution. 2004;46:679–698.

80. Witte H, Moreno E, Rödelsperger C, Kim J, Kim JS, Streit A, et al. Gene inactivation using the CRISPR/Cas9 system in the nematode *Pristionchus pacificus*. Development Genes and Evolution. 2015;225:55–62.

81. Ghanta KS, Ishidate T, Mello CC. Microinjection for precision genome editing in *Caenorhabditis elegans*. STAR Protocols. 2021;2:100748.

82. Han Z, Lo WS, Lightfoot JW, Witte H, Sun S, Sommer RJ. Improving transgenesis efficiency and CRISPR-associated tools through codon optimization and native intron addition in *Pristionchus* nematodes. Genetics. 2020;216:947–956.

83. Eren GG, Roca M, Han Z, Lightfoot JW. Genomic integration of transgenes using UV irradiation in *Pristionchus pacificus*. microPublication Biology. 2022;29.

84. Patro R, Duggal G, Love MI, Irizarry RA, Kingsford C. Salmon provides fast and bias-aware quantification of transcript expression. Nature Methods. 2017;14:417–419.

85. Srivastava A, Malik L, Sarkar H, Zakeri M, Almodaresi F, Soneson C, et al. Alignment and mapping methodology influence transcript abundance estimation. Genome Biology. 2020;21:1–29.

86. Gentleman RC, Carey VJ, Bates DM, Bolstad B, Dettling M, Dudoit S, et al. Bioconductor: open software development for computational biology and bioinformatics. Genome Biology. 2004;5:1–16.

87. Love MI, Anders S, Kim V, Huber W. RNA-Seq workflow: gene-level exploratory analysis and differential expression. F1000Research. 2015;4:1070.

88. Lawrence M, Huber W, Pagès H, Aboyoun P, Carlson M, Gentleman R, et al. Software for computing and annotating genomic ranges. PLOS Computational Biology. 2013;9:e1003118.

89. Pagès H, Carlson M, Falcon S, Li N. AnnotationDbi: Manipulation of SQLite-based annotations in Bioconductor. R package version 1.58.0. 2023. Available from: https://bioconductor.org/packages/release/bioc/html/AnnotationDbi.html

90. Stephens M. False discovery rates: a new deal. Biostatistics. 2017;18:275–294.

91. Rich JT, Neely JG, Paniello RC, Voelker CC, Nussenbaum B, Wang EW. A practical guide to understanding Kaplan-Meier curves. Otolaryngology—Head and Neck Surgery. 2010;143:331–336.

92. Dey T, Lipsitz SR, Cooper Z, Trinh QD, Krzywinski M, Altman N. Regression modeling of time-to-event data with censoring. Nature Methods. 2022;19:1513–1515.

93. Therneau T. A package for survival analysis in R. R package version 3.5-5. 2023. Available from: https://cran.r-project.org/web/packages/survival/index.html

94. Sjoberg D, Baillie M, Haesendonckx S, Treis T. ggsurvfit: Flexible Time-to-Event Figures. R package version 0.3.0. 2023. Available from: http://www.danieldsjoberg.com/ggsurvfit/

95. Kassambara A, Kosinski M, Biecek P, Fabian S. survminer: Drawing Survival Curves using 'ggplot2.' R package version 0.4.9. 2023. Available from: https://cran.r-project.org/web/packages/survminer/index.html

96. Daniel d S, Whiting K, Curry M, Lavery JA, Larmarange J. Reproducible summary tables with the gtsummary package. The R Journal. 2021;13:570–580.

97. Ghedin E, Wang S, Spiro D, Caler E, Zhao Q, Crabtree J, et al. Draft genome of the filarial nematode parasite *Brugia malayi*. Science. 2007;317:1756–1760.

98. Dayi M, Sun S, Maeda Y, Tanaka R, Yoshida A, Tsai IJ, et al. Nearly complete genome assembly of the pinewood nematode *Bursaphelenchus xylophilus* strain Ka4C1. Microbiology Resource Announcements. 2020;9:e01002-20.

99. Srinivasan J, Dillman AR, Macchietto MG, Heikkinen L, Lakso M, Fracchia KM, et al. The draft genome and transcriptome of *Panagrellus redivivus* are shaped by the harsh demands of a free-living lifestyle. Genetics. 2013;193:1279–1295.

100. Gonzalez de la Rosa PM, Thomson M, Trivedi U, Tracey A, Tandonnet S, Blaxter M. A telomere-to-telomere assembly of *Oscheius tipulae* and the evolution of rhabditid nematode chromosomes. G3: Genes, Genomes, Genetics. 2021;11:jkaa020.

101. Stevens L, Moya ND, Tanny RE, Gibson SB, Tracey A, Na H, et al. Chromosome-level reference genomes for two strains of *Caenorhabditis briggsae*: an improved platform for comparative genomics. Genome Biology and Evolution. 2022;14:evac042.

102. Laing R, Kikuchi T, Martinelli A, Tsai IJ, Beech RN, Redman E, et al. The genome and transcriptome of *Haemonchus contortus*, a key model parasite for drug and vaccine discovery. Genome Biology. 2013;14:1–16.

103. Prabh N, Roeseler W, Witte H, Eberhardt G, Sommer RJ, Rödelsperger C. Deep taxon sampling reveals the evolutionary dynamics of novel gene families in *Pristionchus* nematodes. Genome Research. 2018;28:1664–1674.

104. Röseler W, Collenberg M, Yoshida K, Lanz C, Sommer RJ, Rödelsperger C. The improved genome of the nematode *Parapristionchus giblindavisi* provides insights into lineage-specific gene family evolution. G3: Genes, Genomes, Genetics. 2022;12:jkac215.

105. Rödelsperger C, Meyer JM, Prabh N, Lanz C, Bemm F, Sommer RJ. Single-molecule sequencing reveals the chromosome-scale genomic architecture of the nematode model organism *Pristionchus pacificus*. Cell Reports. 2017;21:834–844.

106. Athanasouli M, Witte H, Weiler C, Loschko T, Eberhardt G, Sommer RJ, et al. Comparative genomics and community curation further improve gene annotations in the nematode *Pristionchus pacificus*. BMC Genomics. 2020;21:1–9.

107. Katoh K, Standley DM. MAFFT multiple sequence alignment software version 7: improvements in performance and usability. Molecular biology and evolution. 2013;30:772–780.

108. Schliep KP. phangorn: phylogenetic analysis in R. Bioinformatics. 2011;27:592–593.

109. Mistry J, Finn RD, Eddy SR, Bateman A, Punta M. Challenges in homology search: HMMER3 and convergent evolution of coiled-coil regions. Nucleic Acids Research. 2013;41:e121.

110. Emms DM, Kelly S. OrthoFinder: phylogenetic orthology inference for comparative genomics. Genome Biology. 2019;20:1–14.

111. Karp X. Working with dauer larvae. In: The *C. elegans* research community, editor. WormBook: The Online Review of *C. elegans* Biology. 2018.

112. Anderson MJ. A new method for non-parametric multivariate analysis of variance. Austral Ecology. 2001;26:32–46.

113. Anderson MJ. Permutational multivariate analysis of variance (PERMANOVA). In: Balakrishnan N Colton T, Everitt B, Piegorsch W, Ruggeri F, Teugels JL, editors. Wiley Statsref: Statistics Reference Online. 2017. pp. 1–15.

114. Collyer ML, Adams DC. RRPP: An r package for fitting linear models to high-dimensional data using residual randomization. Methods in Ecology and Evolution. 2018;9:1772–1779.

115. Collyer M, Adams D. RRPP: linear model evaluation with randomized residuals in a permutation procedure. R package version 1.3.1. 2023. Available from: https://cran.r-project.org/web/packages/RRPP/index.html

116. Wickham H, Averick M, Bryan J, Chang W, McGowan LD, François R, et al. Welcome to the Tidyverse. Journal of Open Source Software. 2019;4:1686.

117. Kolde R, Kolde MR. Package 'pheatmap.' R package version 1.0.12. 2023. Available from: https://cran.r-project.org/web/packages/pheatmap/index.html

118. Crameri F, Shephard GE, Heron PJ. The misuse of colour in science communication. Nature Communications. 2020;11:5444.

119. Pedersen TL, Crameri F. Scico: Colour palettes based on the scientific colour-maps. R package version 1.4.0. 2023. Available from: https://cran.r-project.org/web/packages/scico/index.html

120. Garnier S, Ross N, Rudis R, Camargo PA, Sciaini M, Scherer C. viridis—colorblind-friendly color maps for R. R package version 0.6.3. 2023. Available from: https://sjmgarnier.github.io/viridis/

Figures

Fig 1. Phenotypic plasticity throughout the *Pristionchus pacificus* life cycle and the NHR-1/-10/-40 phylogeny. (A) Alternative adult mouth forms in *P. pacificus*. Eu = eurystomatous, St = stenostomatous. (B) *P. pacificus* life cycle, including the alternative "indirect life cycle" via dauer development. (C) Closed mouth morphology of dauer larvae. bp = buccal plug. (D) Maximum-likelihood tree representing the protein phylogeny of NHR-1, NHR-10, and NHR-40 across various nematode species, representing clades III-V. Nodes without dots have a bootstrap support of ≤70%. Bma = *Brugia malayi*, Bxy = *Bursaphelenchus xylophilus*, Cel = *Caenorhabditis elegans*, Cbr = *Caenorhabditis briggsae*, Hco = *Haemonchus contortus*, Mja = *Micoletzkya japonica*, Oti = *Oscheius tipulae*, Pgi = *Parapristionchus giblindavisi*, Ppa = *Pristionchus pacificus*, Pre = *Panagrellus redivivus*.

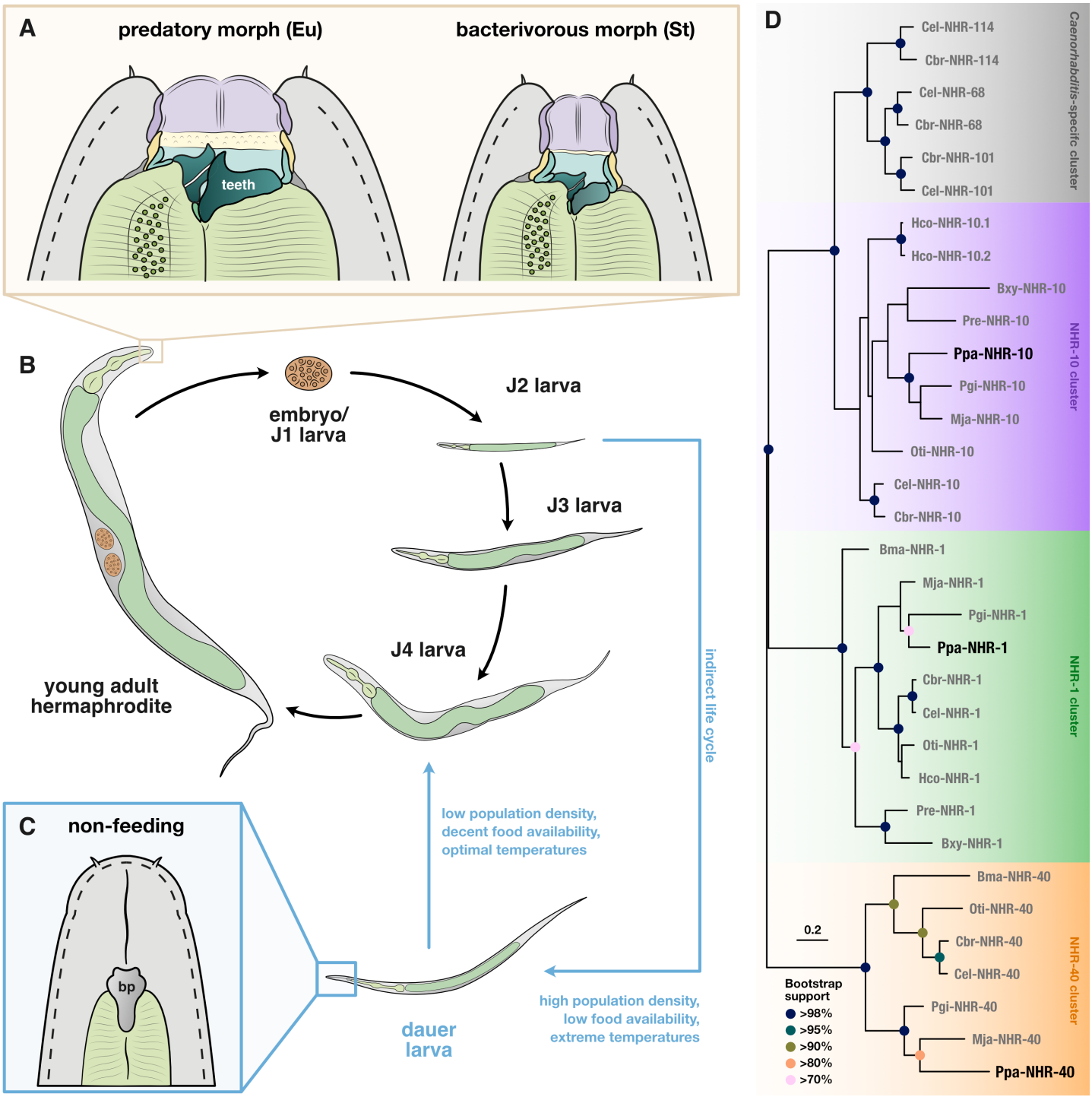
A
predatory morph (Eu)
bacterivorous morph (St)
teeth
B
embryo/
J1 larva
J2 larva
J3 larva
J4 larva
young adult
hermaphrodite
indirect life cycle
low population density,
decent food availability,
optimal temperatures
high population density,
low food availability,
extreme temperatures
dauer
larva
C
non-feeding
bp
D
Caenorhabditis-specific cluster
Cel-NHR-114
Cbr-NHR-114
Cel-NHR-68
Cbr-NHR-68
Cbr-NHR-101
Cel-NHR-101
NHR-10 cluster
Hco-NHR-10.1
Hco-NHR-10.2
Bxy-NHR-10
Pre-NHR-10
Ppa-NHR-10
Pgi-NHR-10
Mja-NHR-10
Oti-NHR-10
Cel-NHR-10
Cbr-NHR-10
NHR-1 cluster
Bma-NHR-1
Mja-NHR-1
Pgi-NHR-1
Ppa-NHR-1
Cbr-NHR-1
Cel-NHR-1
Oti-NHR-1
Hco-NHR-1
Pre-NHR-1
Bxy-NHR-1
NHR-40 cluster
Bma-NHR-40
Oti-NHR-40
Cbr-NHR-40
Cel-NHR-40
Pgi-NHR-40
Mja-NHR-40
Ppa-NHR-40
0.2
Bootstrap support
>98%
>95%
>90%
>80%
>70%

1355
1356

1357
1358 **Fig 2. Patterns of *Ppa-nhr-10* expression across tissues.** A 1.5kb long promoter sequence of
1359 *Ppa-nhr-10* (starting right before the start codon) was fused with *Ppa*-optimzed *GFP*. Relative
1360 strength of fluorescent-protein expression is indicated via a relative intensity scale. (A) and
1361 (B) each show a representative worm from our two independent reporter lines in different
1362 orientations: (A) right body side facing reader, (B) left body side facing reader. Asterisk (*)
1363 in (A) indicates the position of anterior gonad arm. Note that both, anterior and posterior
1364 gonad arms, are always reporting; absence of the anterior arm in (A) is due to image
1365 stacking only. The crossed double-arrows with letters in (A) and (B) indicate anatomical
1366 orientation of the worm: A = anterior, P = posterior, D = dorsal, V = ventral. (C) Zoom-in
1367 on the head of the worm depicted in (B), merged with DIC image. (D) Zoom-in on the
1368 anterior gonad arm (outlined with white dots) of the worm depicted in (B). Note that neither
1369 the sperm cells nor the eggs are reporting *Ppa-nhr-10* expression; only the somatic gonad
1370 tissues do so. amp = ampulla of the gland cell(s), g1D = dorsal pharyngeal gland, g1V =
1371 ventral pharyngeal glands, sp = sperm.
1372

1373

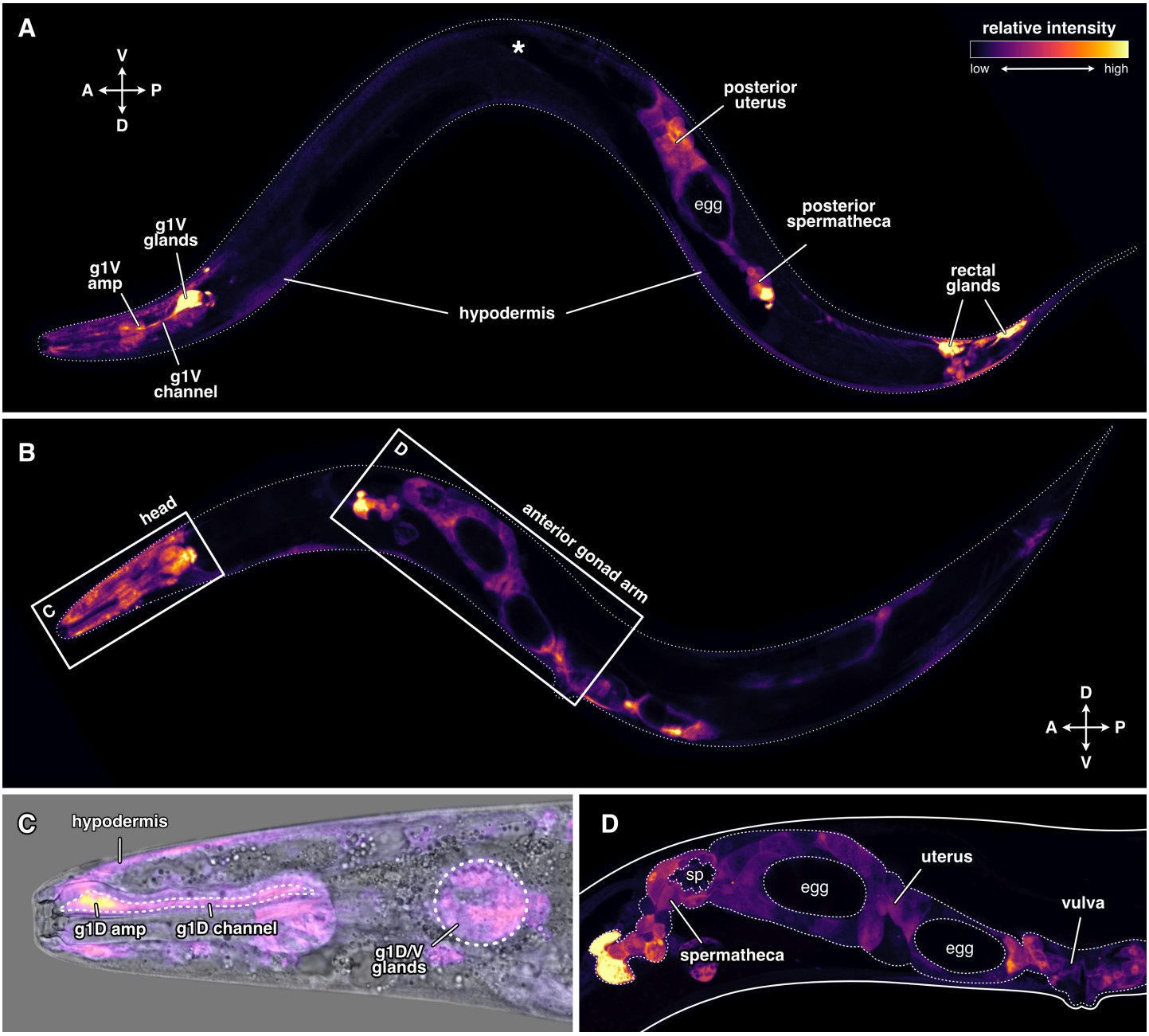
A
V
A
P
D
relative intensity
low
high
*
posterior uterus
egg
posterior spermatheca
g1V glands
g1V amp
hypodermis
rectal glands
g1V channel
B
head
C
D
anterior gonad arm
D
A
P
V
C
hypodermis
g1D amp
g1D channel
g1D/V glands
D
sp
egg
uterus
vulva
spermatheca
egg

1374

1375 **Fig 3. Loss of *nhr-10* does not affect mouth morphology and only weakly affects mouth-**
1376 **form plasticity.** (A) Gene models of *Ppa-nhr-10* and frameshift alleles which lead to early
1377 truncation of the ligand-binding domain. e = exon. (B) Ratio of predatory (Eu) and
1378 bacterivorous (St) animals in the population. Worms were raised and scored on agar plates
1379 with *E. coli* OP50 as a food source. Three biological replicates were obtained (N=3) and 150
1380 worms of each strain were scored per replicate. Significant differences are indicated in black,
1381 non-significant ones in gray. *Z*-scoes and *P*-values were derived from a two-tailed
1382 PERMANOVA with null model residual randomization (RRPP). Bars represent mean
1383 values across all replicates; error bars indicate ±1 standard error of the mean (C) Geometric
1384 morphometric analysis of form differences in the nematode mouths. The PCA plot shows
1385 the distribution of mouth morphologies of individual worms in a form space. Note that the
1386 ranges of morphological variation (outlined by convex hulls) in *Ppa-nhr-10* mutant strains
1387 completely overlap with the wild-type range of morphological variation. (D) Unsupervised
1388 (model-based) clustering reveals that all 144 individuals belong to a single morphological
1389 cluster, demonstrating that mutant worms cannot be differentiated from wild-type worms
1390 based on mouth morphology. Only predatory (Eu) animals were used for the analyses in
1391 (C) and (D).

1392

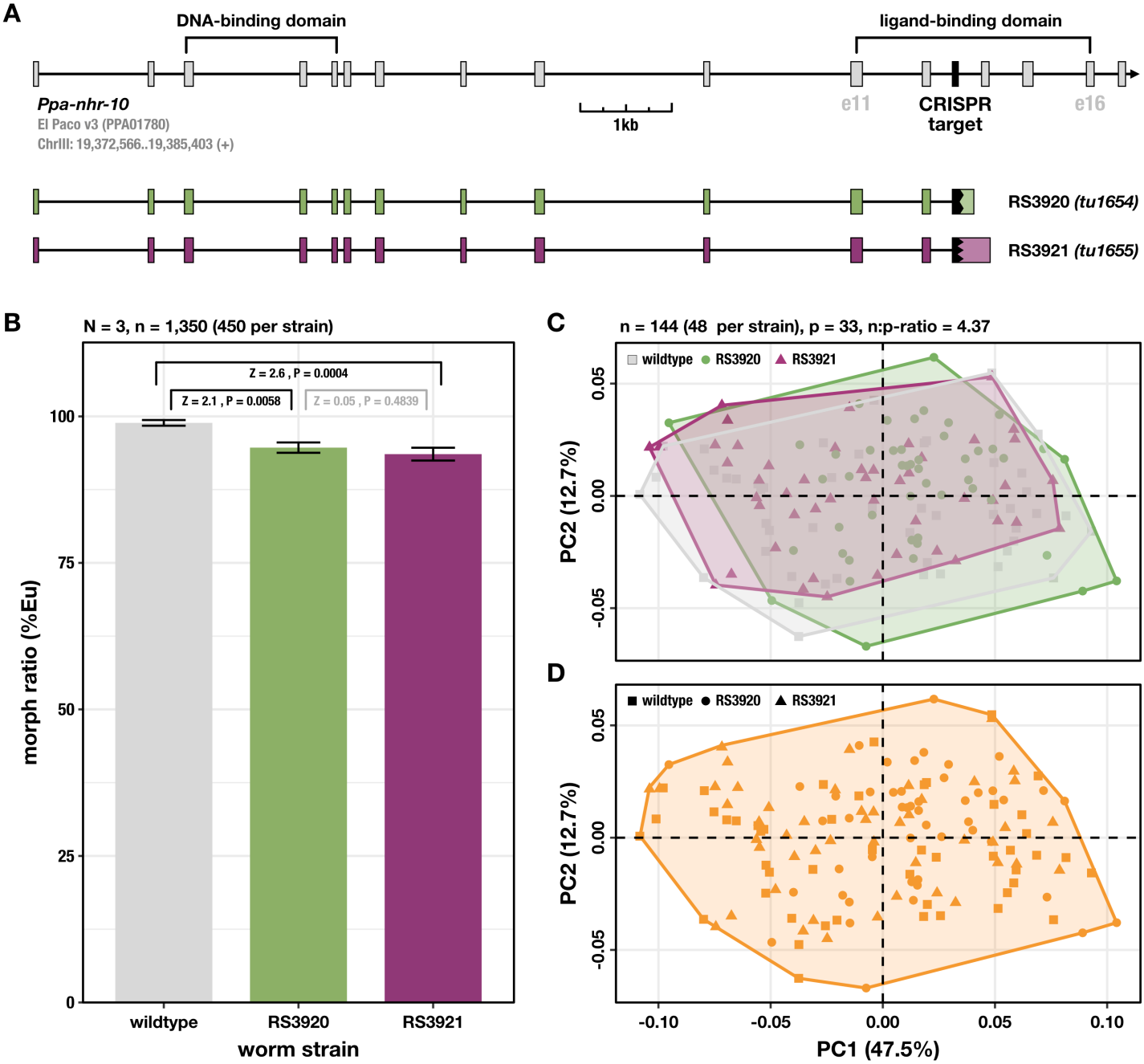

1393

1394

1395 **Fig 4. Loss of *nhr-10* affects expression levels of 32 potential regulatory target genes.** Bold
1396 names along the y-axis correspond to names of the misregulated putative targets
1397 (El_Paco_v3). Target genes which have an exact *C. elegans* ortholog were additionally given
1398 the public gene name of this ortholog (indicated in brackets). Panels indicate in which life
1399 history stage the putative targets genes were found. Labels within the panels indicate
1400 function information for the gene in form of WormCat terms (black) and/or predicted
1401 PFAM domains (gray). WormCat annotations were adapted from *C. elegans,* based on *Cel-*
1402 *Ppa*-orthogroups identified with OrthoFinder. PFAM domains were only indicated for
1403 genes we could not assign a WormCat term to, or genes whose WormCat terms ended in
1404 "unassigned". Cutoffs used in the differential gene expression analysis with DESeq2 and
1405 for PFAM domain prediction with HMMER are indicated in the lower left. DEGs =
1406 differentially expressed genes, MMSE = minimum mean squared error, FSOS = false sign or
1407 smaller.

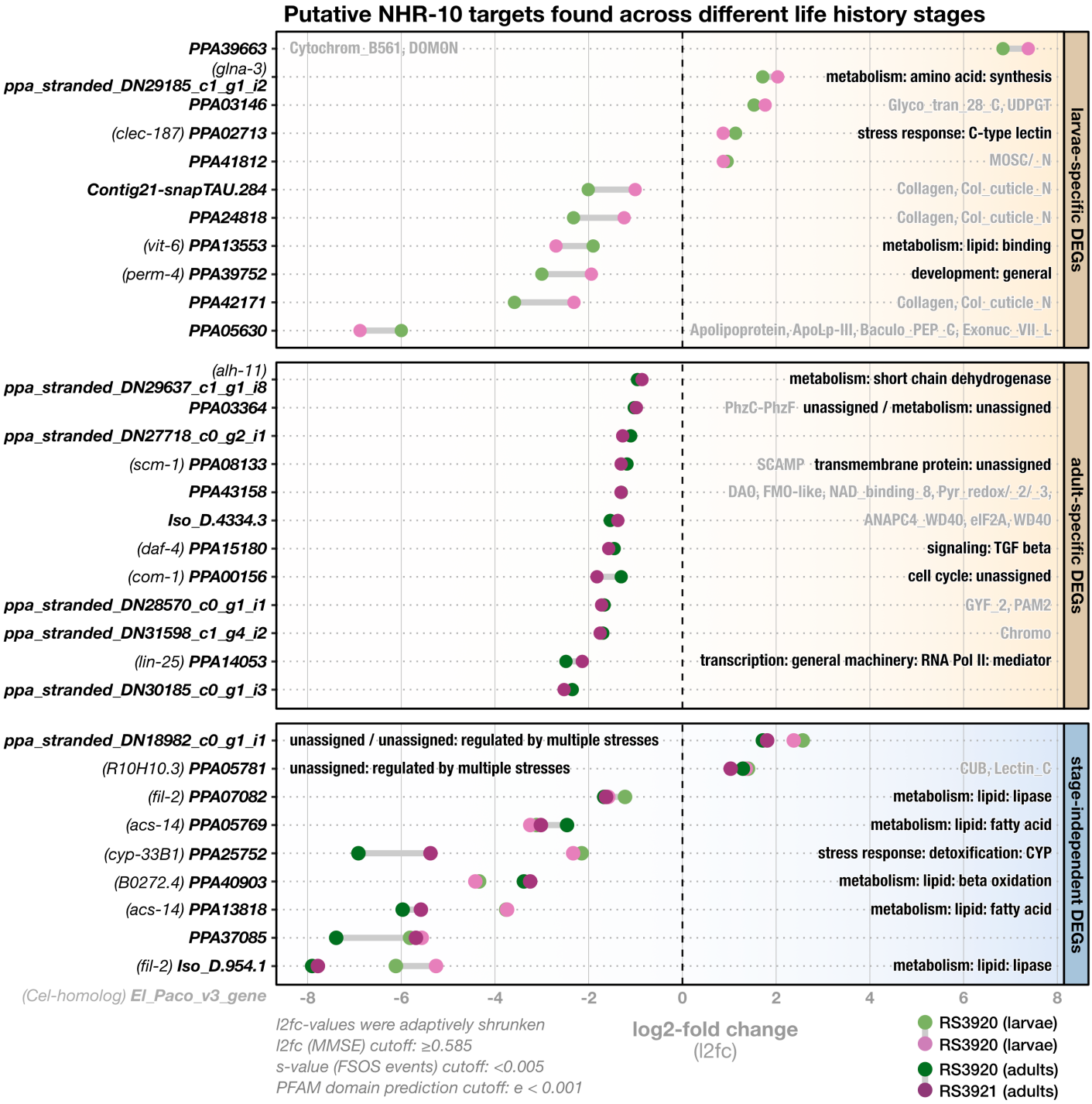

1408

1409

1410

1411

1412
1413 **Fig 5. Survival analyses reveal that the loss of *nhr-10* causes premature death during acute**
1414 **starvation.** Comparison of the overall survival curves of wild-type *P. pacififcus* and two *Ppa-*
1415 *nhr-10(lof)* mutants that were well-fed (A) and completely starved (B). Survival curves show
1416 the mean survival, across all replicates, over time. Transparent ribbons behind the curves
1417 indicate the associated uncertainty in form of ±1 standard errors of the mean. Each of the
1418 two experiments (A and B) was repeated four times independently (N=4); the total numbers
1419 of worms (n) that were tracked across all replicates are indicated on top of both plots.
1420 Indicated *P*-values for pairwise comparisons resulted from a log-rank test that followed a
1421 Kaplan-Meier survival probability estimation; bold and black font indicates significant
1422 differences in the pairwise comparisons of overall survival. (C) Summary of the global
1423 Kaplan-Maier statistics for both experiments (in gray boxes) next to results from Cox
1424 proportional hazard regressions (white boxes). Points indicate the estimated hazard ratios
1425 for both mutant strains within each experiment (relative to the wild-type reference level of
1426 "1.0"). Intervals indicate associated uncertainty in form of 95% confidence intervals. *P*-
1427 values in bold black indicate significant differences between the mutant strain and the
1428 wildtype.
1429
1430

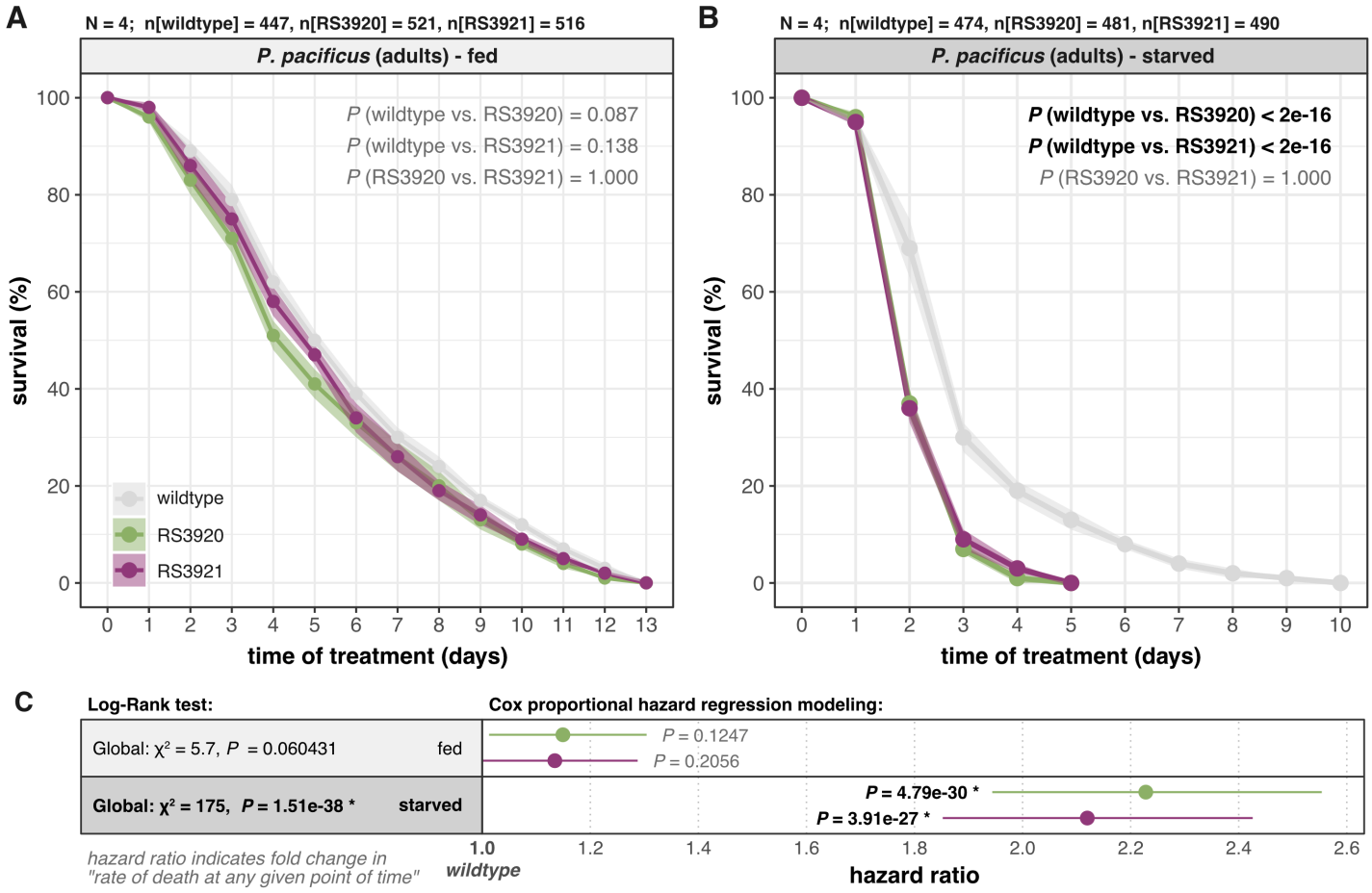

1431

1432

1433

1434
1435 **Fig 6. Analysis of the genome-wide patterns of transcriptional responses to acute**
1436 **starvation in wild-type *P. pacificus*.** (A) Hierarchically clustered heat map showing the
1437 1,007 genes which were identified as differentially expressed in response to 24h of acute
1438 starvation (SRGs). Trees on the left and the top show clustering results based on similarity
1439 in expression levels. Numbers on the gene tree indicate the number of genes in each of the
1440 two response clusters. WT = wildtype. (B) Bar chart showing the overrepresented gene-age
1441 classes and co-expression networks (according to [46]) identified the two response clusters,
1442 relative to the genome. "Phylogenetically old genes" refers to those genes in the genome of
1443 *P. pacificus* which are not diplogastrid-specific orphan genes. (C) Lollipop plot showing
1444 overrepresented PFAM domains in each response cluster. Y-axis gives PFAM domain
1445 names. X-axis gives the percentage of all unique genes encoding this PFAM domain, which
1446 were found to be present in the response cluster (e.g 60% means that 60% all unique genes
1447 in the genome that encode this domain are present in that cluster). (D) Bubble chart showing
1448 overrepresented WormCat terms in each of the response clusters. Enriched categories were
1449 broken down hierarchically (see WormCat legend in the upper right). Bubble size scales
1450 with the gene count indicated to the right of the bubble. The significance scale (q-value)
1451 depicted in (C) also applies to the bubbles depicted in (D).
1452

1453

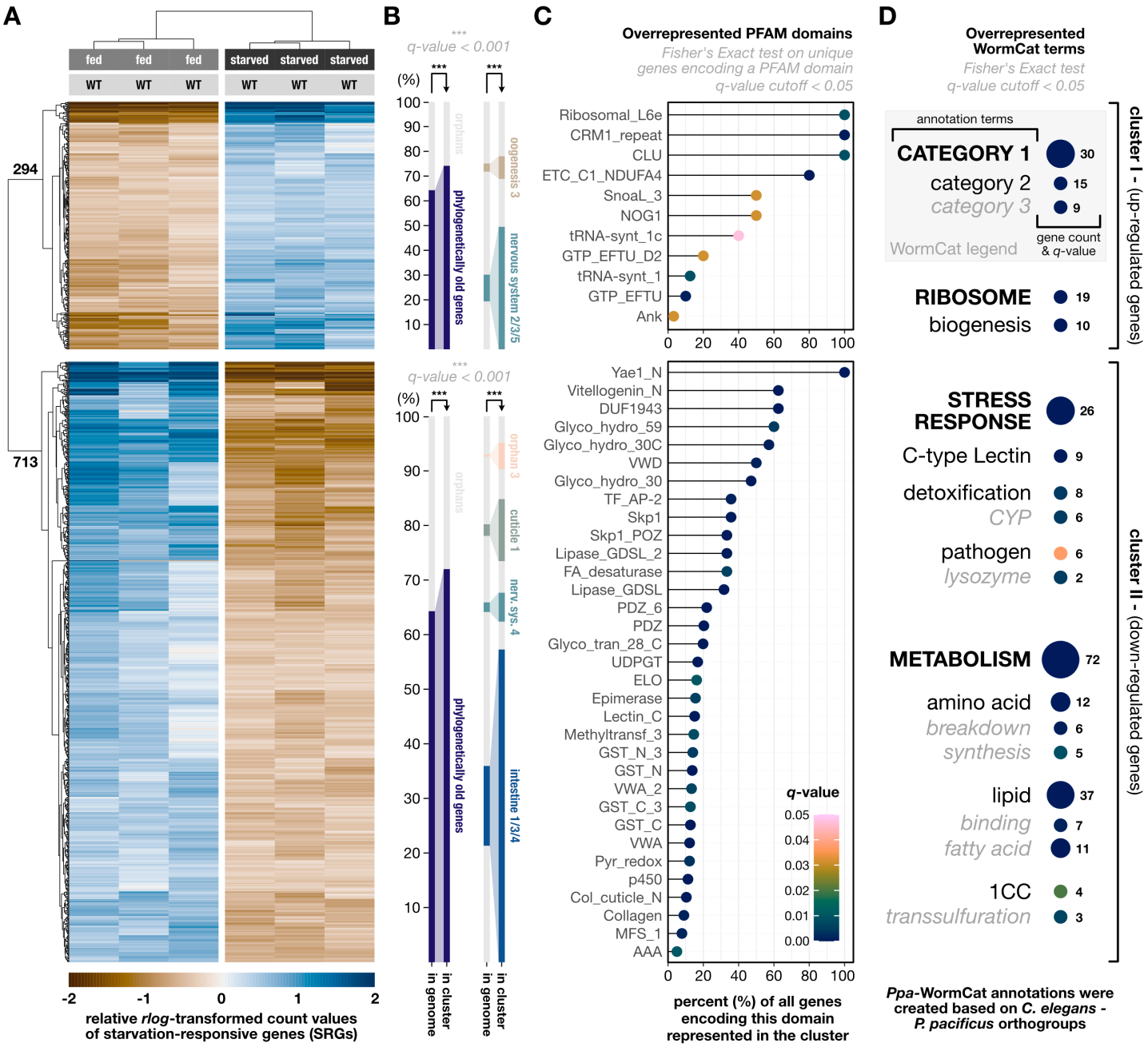
A
fed
fed
fed
starved
starved
starved
WT
294
713
-2
-1
0
1
2
relative rlog-transformed count values of starvation-responsive genes (SRGs)
B
q-value < 0.001
(%)
orphans
phylogenetically old genes
oogenesis 3
nervous system 2/3/5
orphan 3
cuticle 1
nerv. sys. 4
intestine 1/3/4
in genome
in cluster
C
Overrepresented PFAM domains
Fisher's Exact test on unique genes encoding a PFAM domain
q-value cutoff < 0.05
Ribosomal_L6e
CRM1_repeat
CLU
ETC_C1_NDUFA4
SnoaL_3
NOG1
tRNA-synt_1c
GTP_EFTU_D2
tRNA-synt_1
GTP_EFTU
Ank
Yae1_N
Vitellogenin_N
DUF1943
Glyco_hydro_59
Glyco_hydro_30C
VWD
Glyco_hydro_30
TF_AP-2
Skp1
Skp1_POZ
Lipase_GDSL_2
FA_desaturase
Lipase_GDSL
PDZ_6
PDZ
Glyco_tran_28_C
UDPGT
ELO
Epimerase
Lectin_C
Methyltransf_3
GST_N_3
GST_N
VWA_2
GST_C_3
GST_C
VWA
Pyr_redox
p450
Col_cuticle_N
Collagen
MFS_1
AAA
q-value
0.05
0.04
0.03
0.02
0.01
0.00
percent (%) of all genes encoding this domain represented in the cluster
D
Overrepresented WormCat terms
Fisher's Exact test
q-value cutoff < 0.05
annotation terms
CATEGORY 1
category 2
category 3
WormCat legend
gene count & q-value
RIBOSOME
biogenesis
STRESS RESPONSE
C-type Lectin
detoxification
CYP
pathogen
lysozyme
METABOLISM
amino acid
breakdown
synthesis
lipid
binding
fatty acid
1CC
transsulfuration
cluster I - (up-regulated genes)
cluster II - (down-regulated genes)
Ppa-WormCat annotations were created based on C. elegans - P. pacificus orthogroups

1454

1455

1456 **Fig 7. Loss of *nhr-10* disturbs the expression levels of 37 putative regulatory targets in**
1457 **starving worms.** Bold names along the y-axis correspond to names of the misregulated
1458 putative targets (El Paco v3) which are likely to cause the observed starvation-survival
1459 phenotype. Genes which have an exact *C. elegans* ortholog were additionally given the
1460 public gene name of this ortholog (indicated in brackets). Panels indicate whether these
1461 targets are members of the SRGs or not. Labels within the panels indicate functional
1462 information for the gene in form of WormCat terms (black) and/or predicted PFAM
1463 domains (gray). WormCat annotations were adapted from *C. elegans,* based on *Cel-Ppa-*
1464 orthogroups identified with OrthoFinder. PFAM domains were only indicated for genes we
1465 could not assign a WormCat term to, or genes whose WormCat terms ended in
1466 "unassigned". Cutoffs used in the differential gene expression analysis with DESeq2 and
1467 for PFAM domain prediction with HMMER are indicated in the lower left. Note that, in the
1468 current El Paco v3 annotations, PPA25752 (in SRG targets) seems to be a gene model that
1469 artificially fuses two separate genes. This is supported by multiple available RNA datasets
1470 and our PFAM domain predictions, which revealed that the first half of the hypothetical
1471 protein encodes a 7TM_GPCR, while the second half encodes a p450 cytochrome. As it
1472 seems unlikely that a single protein would act as both, a GPCR and a cytochrome, we
1473 repeated our differential expression analysis after manually splitting PPA25752 into two
1474 separate genes. We found no evidence of differential expression for the resulting GPCR-
1475 gene, but could perfectly replicate the differential expression signature we originally found
1476 for PPA25752, for the cytochrome-encoding gene. FSOS = false sign or smaller, MMSE =
1477 minimum mean squared error, SRG = starvation-response gene.

1478

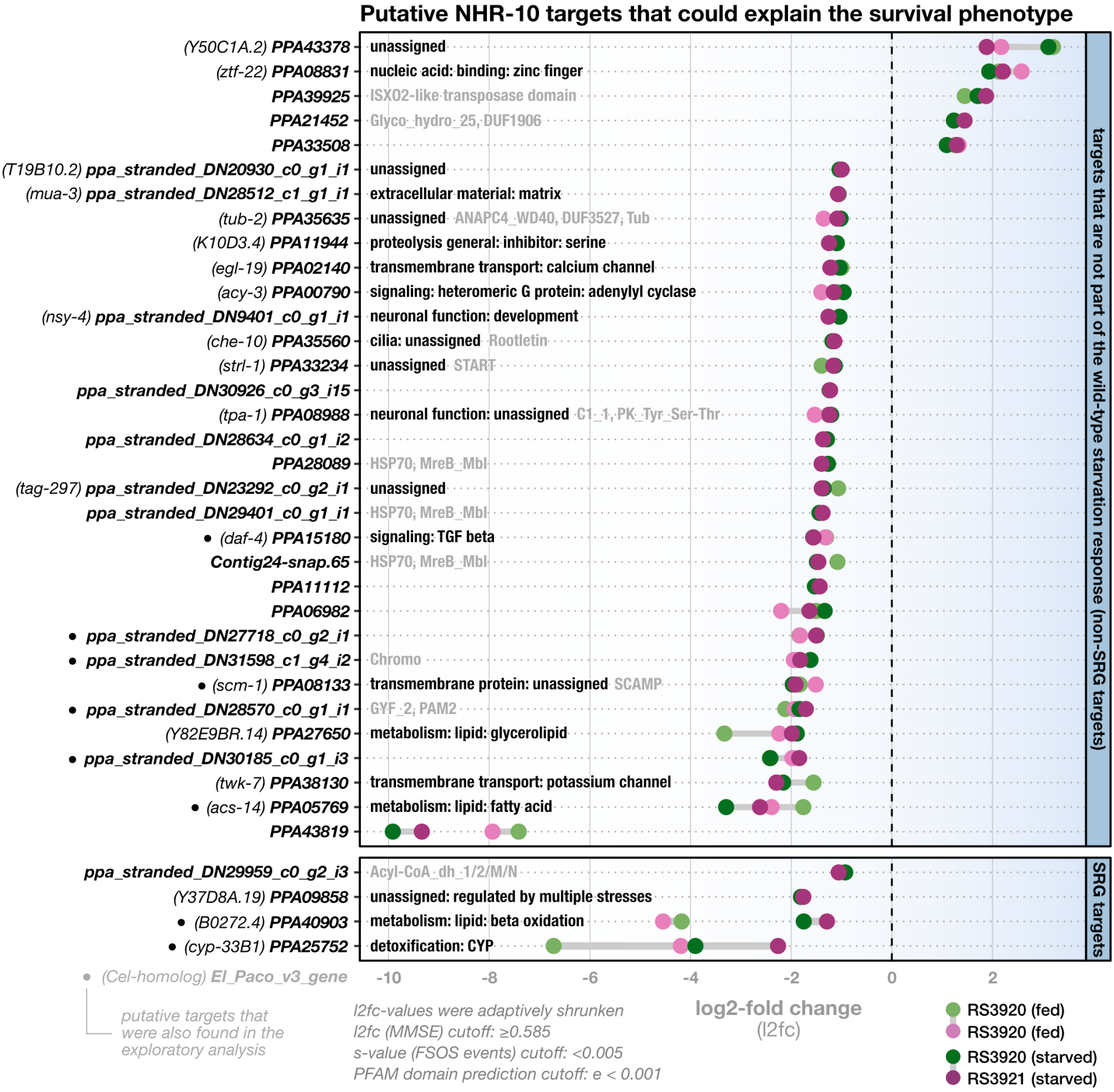

1479

1480

1481 **Fig 8. Loss of *nhr-10* also causes various dauer-related phenotypes, including impaired**
1482 **long-term survival.** (A). Workflow of the three dauer assays. (B-D) Results of the individual
1483 phenotypic assays indicated above each plot in the workflow chart. Point ranges indicate
1484 the mean estimates across all replicates ±1 standard error of the mean. Note that the dauers
1485 used in the exit and survival assays (C-D) were obtained from LCs without cholesterol.
1486 Additionally, all of the worms in (C) managed to exit dauer and fully resumed
1487 developments into viable adults. Hypothesis tests used a two-tailed PERMANOVA with
1488 null model residual randomization (RRPP); relative effect sizes (*Z*-scores) and *P*-values for
1489 pairwise comparisons among the three strains are reported in the upper right of each panel.
1490 Incompatibility with the null hypothesis ($Z \geq 2$ and $P < 0.05$) indicates the presence of a
1491 strain-specific phenotype; compatibility with the null hypothesis ($Z < 2$ or $P \geq 0.05$) supports
1492 the absence of a strain-specific phenotype. LCs = liquid cultures, rpm = rotations per
1493 minute, SDS = sodium dodecyl sulfate, SEM = standard error of the mean. All experiments
1494 were repeated multiple times independently (N=4). Number of worms in (B): n[PS312, (-)]
1495 = 460; n[RS3920, (-)] = 537; n[RS3921, (-)] = 432; n[PS312, (+)] = 750; n[RS3920, (+)] = 877;
1496 n[RS3921, (+)] = 879. Number of worms in (C): n[PS312] = 240; n[RS3920] = 240; n[RS3921]
1497 = 240. Number of worms in (D): n[PS312] = 395; n[RS3920] = 175; n[RS3921] = 177.

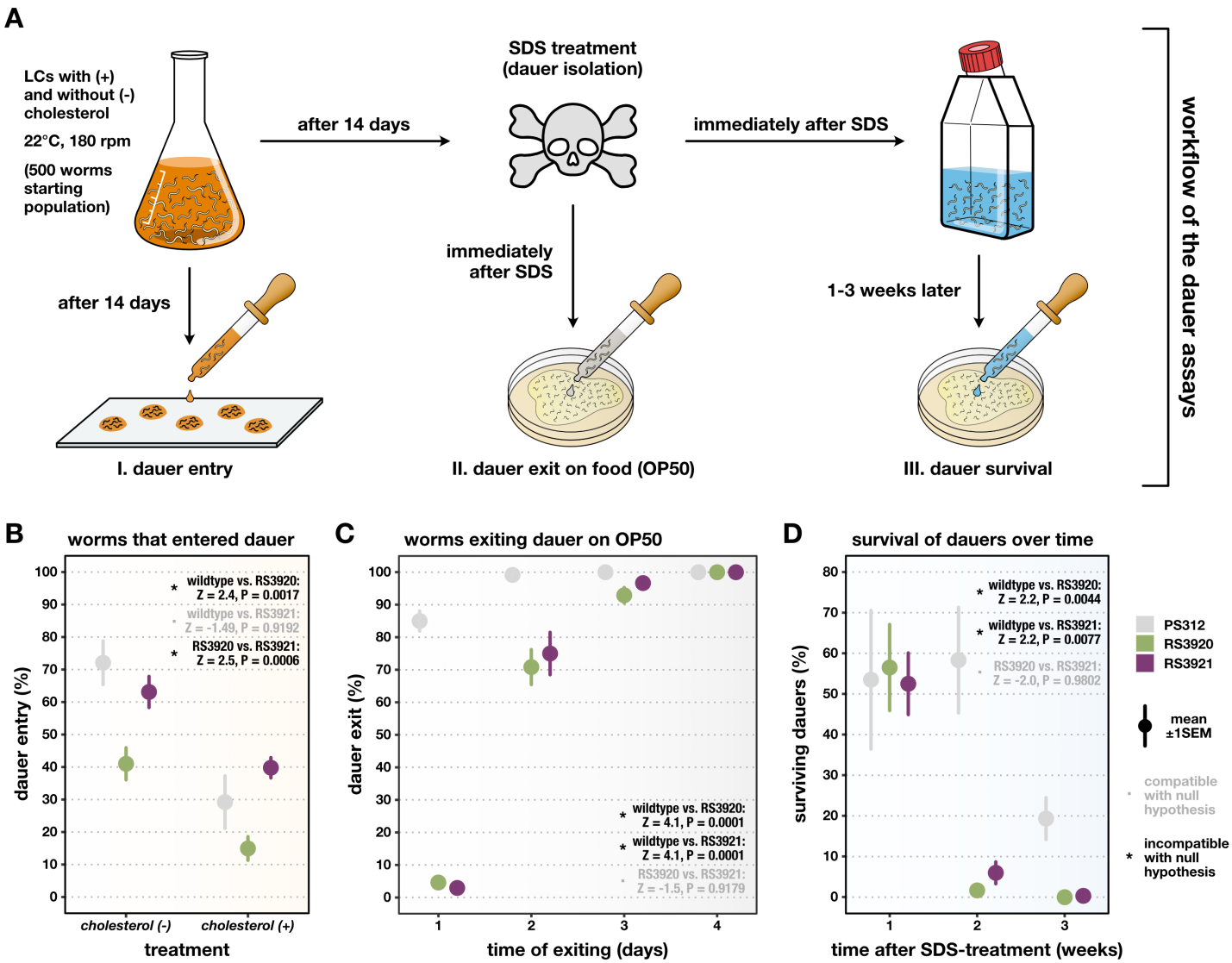
A
LCs with (+) and without (-) cholesterol
22°C, 180 rpm
(500 worms starting population)
after 14 days
SDS treatment (dauer isolation)
immediately after SDS
after 14 days
immediately after SDS
1-3 weeks later
I. dauer entry
II. dauer exit on food (OP50)
III. dauer survival
workflow of the dauer assays
B
worms that entered dauer
wildtype vs. RS3920: Z = 2.4, P = 0.0017
wildtype vs. RS3921: Z = -1.49, P = 0.9192
RS3920 vs. RS3921: Z = 2.5, P = 0.0006
dauer entry (%)
cholesterol (-)
cholesterol (+)
treatment
C
worms exiting dauer on OP50
wildtype vs. RS3920: Z = 4.1, P = 0.0001
wildtype vs. RS3921: Z = 4.1, P = 0.0001
RS3920 vs. RS3921: Z = -1.5, P = 0.9179
dauer exit (%)
time of exiting (days)
D
survival of dauers over time
wildtype vs. RS3920: Z = 2.2, P = 0.0044
wildtype vs. RS3921: Z = 2.2, P = 0.0077
RS3920 vs. RS3921: Z = -2.0, P = 0.9802
surviving dauers (%)
time after SDS-treatment (weeks)
PS312
RS3920
RS3921
mean ±1SEM
compatible with null hypothesis
incompatible with null hypothesis

Supplementary Information

Sup Fig 1. Heatmap showing relative expression levels of NHR-10's regulatory targets from the confirmatory RNA-seq experiment. Hierarchical clustering was performed on the relative *rlog*-transformed normalized count values of the 37 genes which were identified as differentially expressed in mutants that have been acutely starved (see Fig 7 in main text). Trees on the left and the top show clustering results based on similarity in expression levels. Hierarchical clustering of all transcriptome samples based on the 37 candidate genes alone, perfectly recovered the grouping structures of the experiment (i.e., wildtype *vs.* mutant and fed *vs.* starved).

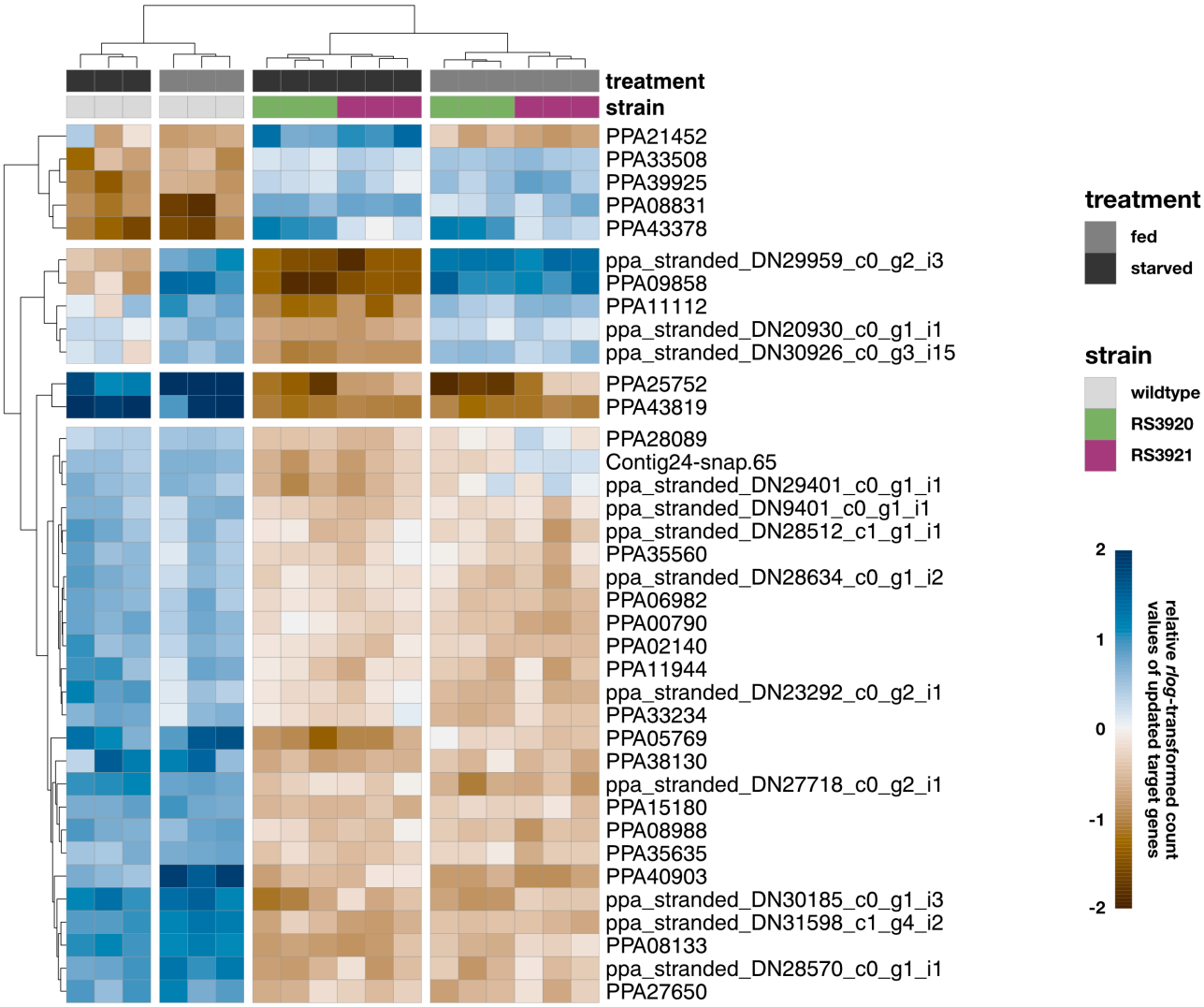
treatment
strain
PPA21452
PPA33508
PPA39925
PPA08831
PPA43378
ppa_stranded_DN29959_c0_g2_i3
PPA09858
PPA11112
ppa_stranded_DN20930_c0_g1_i1
ppa_stranded_DN30926_c0_g3_i15
PPA25752
PPA43819
PPA28089
Contig24-snap.65
ppa_stranded_DN29401_c0_g1_i1
ppa_stranded_DN9401_c0_g1_i1
ppa_stranded_DN28512_c1_g1_i1
PPA35560
ppa_stranded_DN28634_c0_g1_i2
PPA06982
PPA00790
PPA02140
PPA11944
ppa_stranded_DN23292_c0_g2_i1
PPA33234
PPA05769
PPA38130
ppa_stranded_DN27718_c0_g2_i1
PPA15180
PPA08988
PPA35635
PPA40903
ppa_stranded_DN30185_c0_g1_i3
ppa_stranded_DN31598_c1_g4_i2
PPA08133
ppa_stranded_DN28570_c0_g1_i1
PPA27650
treatment
fed
starved
strain
wildtype
RS3920
RS3921
2
1
0
-1
-2
relative rlog-transformed count values of updated target genes

12
13
14

15 **Sup Tab 1. Overrepresentation analysis shows now bias towards any given chromosomal**
16 **location among *Ppa*-NHR-10's targets.** The 37 candidate regulatory targets (DEGs) of *Ppa*-
17 NHR-10, which were identified in the confirmatory RNA-seq experiments, were used as
18 input for the analysis. No significant bias (FDR-corrected *P*-value < 0.05) towards any
19 particular chromosome was found for *Ppa*-NHR-10's target genes. DEG = differentially
20 expressed gene, FDR = false discovery rate.

chromosome	number_of_genes	number_of_DEGs	fold_enrichment	FDR_corrected_pvalue
Chr1	6869	5	0.5684764688986556	0.35319808452624085
Chr2	4462	11	1.9253031606236448	0.13589186241137188
Chr3	3736	5	1.045199374963829	0.9702253905888654
Chr4	6594	10	1.1843690824582545	0.8351614949834785
Chr5	4097	5	0.9531034573748757	1
ChrX	3002	1	0.26015089039739275	0.35319808452624085

21

Sup Tab 2. Loss of *Ppa-nhr-10* does not affect the expression levels of *P. pacificus* orthologs of the *C. elegans* propionate shunt genes. El Paco ver. 3 annotations were used for *P. pacificus*. *s*-values indicate FSOS event probability; significant changes to the expression levels ($s < 0.005$) could not be observed in any case. Strain indicated the *Ppa-nhr-10(lof)* mutant that was compared to wild-type worms. Cel = *C. elegans*, FSOS = false sign or smaller than 50% up- or down-regulated, l2fc = log2-fold change in expression levels, mmse = minimum mean squared error, sd = standard deviation.

Cel_gene	pristionchus_ortholog	l2fc_mmse	l2fc_posterior_sd	s-value	strain	treatment
alh-8	PPA18546	0.3120081894467676	0.183586125982154	0.779593708146979	RS3920	fed
alh-8	PPA18546	0.0700641209645215	0.124433208963777	0.903335595238679	RS3920	starved
alh-8	PPA18546	0.1578326679985086	0.116470311709115	0.870830237769447	RS3921	fed
alh-8	PPA18546	0.1310214980190643	0.111534703830993	0.801497484867020	RS3921	starved
ech-6	ppa_stranded_DN19950_c1_g2_i1	0.2915677450017385	0.121252839902834	0.890590474805354	RS3920	fed
ech-6	ppa_stranded_DN19950_c1_g2_i1	0.0278618218738554	0.058205088196759	0.922220261931968	RS3920	starved
ech-6	ppa_stranded_DN19950_c1_g2_i1	0.302048528212008	0.099893413969880	0.865990199881571	RS3921	fed
ech-6	ppa_stranded_DN19950_c1_g2_i1	0.1002545176406774	0.078147156473995	0.831089635382915	RS3921	starved
hach-1	ppa_stranded_DN24485_c0_g1_i1	0.1503250384307045	0.179955991152806	0.871633632978635	RS3920	fed
hach-1	ppa_stranded_DN24485_c0_g1_i1	-0.003755268928726	0.048962247587748	0.916236852972432	RS3920	starved
hach-1	ppa_stranded_DN24485_c0_g1_i1	0.3403493778772363	0.171220920053186	0.685735755852485	RS3921	fed
hach-1	ppa_stranded_DN24485_c0_g1_i1	-0.029993946051769	0.095674037390754	0.816727072214799	RS3921	starved
hphd-1	PPA05876	0.2710472432776699	0.186482563130857	0.845357698346291	RS3920	fed
hphd-1	PPA05876	-0.021954386415356	0.066963132113470	0.912373249230267	RS3920	starved
hphd-1	PPA05876	0.1715677303340060	0.120611075832775	0.868252620804282	RS3921	fed
hphd-1	PPA05876	-0.388037641153159	0.170339234415574	0.558929874614430	RS3921	starved

29